Science of the Total Environment 757 (2021) 143896

Contents lists available at ScienceDirect

Science of the Total Environment

journal homepage: www.elsevier.com/locate/scitotenv

Untangling mechanisms of crude oil toxicity: Linking gene expression, morphology and PAHs at two developmental stages in a cold-water fish

Elin Sørhus [a,*], Carey E. Donald [a], Denis da Silva [b], Anders Thorsen [a], Ørjan Karlsen [a], Sonnich Meier [a]

[a] Institute of Marine Research, Bergen, Norway
[b] Northwest Fisheries Science Center (NOAA), 2725 Montlake Blvd. East, Seattle, WA 98112-2097, USA

HIGHLIGHTS

- Toxicity to dissolved oil was compounded by oil droplet fouling on the eggshell.
- Exposure early in development resulted in higher PAH uptake due to lower metabolism resulting in more severe abnormalities.
- A rapid and circulation-independent regulation of *bmp10* suggested a direct oil-induced effect on calcium homeostasis.
- Expression of *rhag* indicated a direct oil-induced effect on osmoregulatory cells and osmoregulation.
- Severe eye abnormalities especially in the late exposure was linked to inappropriate overexpression of *cyp1b* in the eyes.

GRAPHICAL ABSTRACT

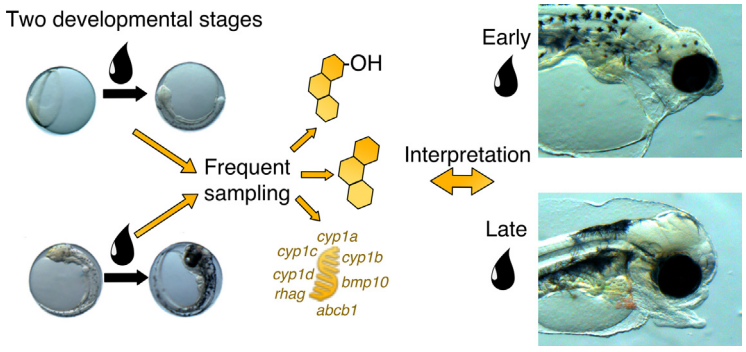

ARTICLE INFO

Article history:
Received 14 September 2020
Received in revised form 17 November 2020
Accepted 17 November 2020
Available online 2 December 2020

Editor: Henner Hollert

Keywords:
Crude oil exposure
PAH uptake and metabolism
gene expression
cyp1a
cyp1b
cyp1c
cyp1d

ABSTRACT

Early life stages of fish are highly sensitive to crude oil exposure and thus, short term exposures during critical developmental periods could have detrimental consequences for juvenile survival. Here we administered crude oil to Atlantic haddock (*Melanogrammus aeglefinus*) in short term (3-day) exposures at two developmental time periods: before first heartbeat, from gastrulation to cardiac cone stage (*early*), and from first heartbeat to one day before hatching (*late*). A frequent sampling regime enabled us to determine immediate PAH uptake, metabolite formation and gene expression changes. In general, the embryotoxic consequences of an oil exposure were more severe in the *early* exposure animals. Oil droplets on the eggshell resulted in severe cardiac and craniofacial abnormalities in the highest treatments. Gene expression changes of Cytochrome 1 a, b, c and d (*cyp1a*, *b*, *c*, *d*), Bone morphogenetic protein 10 (*bmp10*), ABC transporter b1 (*abcb1*) and Rh-associated G-protein (*rhag*) were linked to PAH uptake, occurrence of metabolites of phenanthrene and developmental and functional abnormalities. We detected circulation-independent, oil-induced gene expression changes and separated phenotypes linked to proliferation, growth and disruption of formation events at early and late developmental stages. Changes in *bmp10* expression suggest a direct oil-induced effect on calcium homeostasis. Localized expression of *rhag* propose an impact on osmoregulation. Severe eye abnormalities were linked to possible inappropriate

* Corresponding author.
E-mail address: elins@hi.no (E. Sørhus).

https://doi.org/10.1016/j.scitotenv.2020.143896

bmp10
abcb1
rhag
Two developmental time periods
Atlantic haddock
Phenanthrene metabolites

overexpression of *cyp1b* in the eyes. This study gives an increased knowledge about developmentally dependent effects of crude oil toxicity. Thus, our findings provide more knowledge and detail to new and several existing adverse outcome pathways of crude oil toxicity.

1. Introduction

Globally, fish habitats are frequently impacted by accidental oil spills. For fish, consequences of crude oil toxicity are stage dependent, and early life stages (eggs and larvae) are thought to be highly vulnerable for several reasons. Early life stages drift and have no opportunity to avoid contaminated areas compared to juvenile and mature fish (Carroll et al., 2018; Olsen et al., 2010). Relative content of lipids and surface-area-to-volume ratio are higher in early life stages compared to juveniles/adults, making them more susceptible to accumulation of lipophilic environmental toxicants (Petersen and Kristensen, 1998). Finally, critical developmental processes like patterning and organogenesis can be disrupted by crude oil exposure (Incardona, 2017; Pasparakis et al., 2019; Sørhus et al., 2017). However, there are large interspecies sensitivity differences. The Atlantic haddock (*Melanogrammus aeglefinus*) has a sticky eggshell which adhere oil droplets. Due to this oil droplet fouling, the haddock embryo is approximately 10 times more sensitive to crude oil than its close relative Atlantic cod (*Gadus morhua*) (Sørensen et al., 2017).

Crude oil is a complex mixture of thousands of different components. Multiple toxic components in oil can therefore be responsible for the observed toxicity (Meador and Nahrgang, 2019). Still, the content of polycyclic aromatic hydrocarbons (PAHs) appears to correlate to the toxicity in developing fish (Adams et al., 2014; Carls and Meador, 2009). Metabolism and excretion of the larger PAHs (4–6 rings) is initiated by activation of the aryl hydrocarbon receptor (AhR), which in turn induces xenobiotic biotransformation battery, such as Cytochrome P4501A (CYP1A). CYP1A induction has for a long time been used as a sensitive biomarker for crude oil toxicity (Goksøyr, 1995). The detoxification process is divided into three phases, with activation of substrate in phase I by e.g. CYP1A, followed by conjugation in phase II, and finally transport and excretion in phase III (Wells et al., 2009). Although PAHs are themselves toxic, reactive intermediates (reactive oxygen species, ROS) created during the detoxification process can cause toxicity such as oxidative damage to cellular macromolecules and disruption of signal transduction (Wells et al., 1997).

Cardiac morphology abnormalities due to oil exposure can be a result of AhR-dependent mechanisms (Wells et al., 1997), circulation abnormalities (Andres-Delgado and Mercader, 2016) and direct disruption of signaling pathways, e.g. calcium signaling (Ebert et al., 2005; Incardona, 2017; Rottbauer et al., 2001; Sørhus et al., 2017). In addition, tricyclic PAHs are shown to cause cardiotoxicity through an AhR-independent process (Incardona et al., 2004; Marris et al., 2019). Non-alkylated tricyclic PAHs do not induce AhR (Hawkins et al., 2002), and instead act by blocking the repolarizing potassium efflux and a reduction in intracellular calcium cycling (Brette et al., 2014; Brette et al., 2017). The disruption of ionic signaling leads to defects in cardiac rhythm and contractility (Incardona et al., 2014; Incardona et al., 2009; Sørhus et al., 2016b) as well as calcium regulated cardiomyocyte proliferation (Ebert et al., 2005; Huang et al., 2012; Rottbauer et al., 2001; Sørhus et al., 2017). Beyond these circulatory defects that affect cardiac development (Andres-Delgado and Mercader, 2016), other extra-cardiac abnormalities can be secondary to circulatory defects, including craniofacial and eye development, and osmoregulatory and lipid metabolism deficiencies (Incardona et al., 2004; Incardona and Scholz, 2016; Johann et al., 2020; Laurel et al., 2019; Sørhus et al., 2017; Sun et al., 2019).

Numerous other pathways/endpoints have also been reported beyond the effects downstream of circulatory defects described above. PAH-related disruption of retinoid signaling interrupts eye development (Lie et al., 2019). Craniofacial development and growth can be disrupted by inappropriate signaling in formation processes like midline signaling (Abramyan, 2019; Delling et al., 2013; Kimmel et al., 2001) or secondary to impact on craniofacial muscle apparatus (Shwartz et al., 2012). Severe oil-induced aberrations lead to early larval mortality, yet even the smaller developmental impacts can affect survival later in life (Cresci et al., 2020; Heintz et al., 2000; Hicken et al., 2011). Recently, a study linked oil-induced changes in lipid composition and dynamics to reduced growth and survival in polar cod (*Boreogadus saida*) (Laurel et al., 2019). Consistently, impacts on lipid metabolism pathways have been reported in several RNAseq studies (Sørhus et al., 2017; Xu et al., 2016). Several gene expression studies have started to unravel key events of adverse outcome pathways of crude oil (Laurel et al., 2019; Lie et al., 2019; McGruer et al., 2019; Sørhus et al., 2017; Xu et al., 2019; Xu et al., 2018), but there are still knowledge gaps in understanding the underlying mechanisms of crude oil toxicity.

In this study we aim to improve our understanding of cause and effect relationships by linking immediate transcriptional changes to morphological phenotypes, PAH uptake and metabolism. A frequent and thorough sampling regime during and after exposure enabled us to detect immediate changes. We focused specifically on genes found interesting in a previous study (Sørhus et al., 2017) that are involved in various parts of development and function: cardiac development and calcium homeostasis (Bone morphogenetic protein 10 (*bmp10*)), transport of xenobiotic products (ABC transporter b1 (*abcb1*)), osmoregulation and ammonium waste excretion (Rh-associated G-protein (*rhag*)), and enzymes possibly involved in phase I xenobiotic metabolism (Cytochrome P450 1s (*cyp1a*, *b*, *c*, *d*)).

This study was designed to understand key events of adverse outcome pathways. First, exposure at the early embryonic stage prior to first heartbeat (2.5–5.5 days post-fertilization (dpf)) allowed us to detect circulation-independent, oil-induced gene expression changes. Second, exposure both during and after completion of organogenesis (7.5–10.5 dpf) enabled us to separate phenotypes linked to proliferation, growth and disruption of formation events at early and late developmental stages. Second, we aimed to investigate the contribution of oil droplets to toxicity by positioning eggs both within and underneath the surface oil slick. Finally, increased knowledge about uptake, induction and rate of PAH metabolism helps to pinpoint chemical drivers of crude oil toxicity. A greater understanding of crude oil toxicity in the framework of adverse outcome pathways is essential for predicting more accurately both acute and delayed consequences of accidental oil spills and operational oil releases, such as produced water.

2. Materials and methods

2.1. Animal collection, maintenance and exposure set up

Fertilized Atlantic haddock (*Melanogrammus aeglefinus*) eggs were collected from tanks with wild-caught broodstock haddock maintained at the Institute of Marine Research, Austevoll Research station. The fertilized eggs were kept in indoor incubators (8 ± 1 °C), until transfer of ≈5000 eggs to 50 L green polyethylene plastic experimental tanks. Flow through in the tanks was set to 32 L/h, the water temperature

8.0 °C. The light regime was 12 h light, 12 h dark provided by broad spectrum 2x36W Osram Biolux 965 dimmable fluorescent light tubes (Osram GmbH, Munich, Germany).

The crude oil used was a weathered blend from the Heidrun oil field of the Norwegian sea. The blend was a mixture of 4 different formations that contain different oil types. This included light paraffinic oil (0.83 g/mL) and more heavily degradable oils (0.93 g/mL). The PAHs constituted 2% of the total oil by weight (19.6 g/kg). The crude oil is representative of the oil found in Lofoten island areas, an area of both haddock spawning and potential oil industry development. The exposure regime was identical to previous studies (Sørhus et al., 2015; Sørhus et al., 2016b). In short, the oil was artificially weathered before it was pumped into a dispersion system. The system generated oil droplets in the low μm size range (Nordtug et al., 2011). Exposure concentration to the tanks were regulated by a 3-way magentic valve connected to a parallel pipeline system with sea water and oil solution. Different concentrations into the tanks were achieved by changing the open/close time of the valves.

Two short (72 h) exposure experiments were performed, hereafter referred to as *early* and *late* exposure (Fig. 1A). The *early* exposure started at 2.5 dpf and ended at 5.5 dpf (10% epiboly to 10–20 somite/cardiac cone stage), while the *late* exposure started at 7.5 dpf and ended at 10.5 dpf (30–40 somite stage to hatching gland stage). The experimental setup consisted of a control and three exposure concentrations in a total of 18 tanks (Fig. 1B): control (*C*) 0.0 μg oil/L; low (*L*) 30 μg oil/L; medium (*M*) 100 μg oil/L; and high 300 μg oil/L. In our previous oil exposure experiments with haddock embryos, eggs were allowed to float freely (Sørensen et al., 2017; Sørhus et al., 2015; Sørhus et al., 2016b). Haddock eggs have a natural high buoyancy which propels them close to the surface, where they are potentially exposed to the slick. Therefore, eggs were added to plankton mesh chambers (Fig. 1B) in four replicate tanks of each treatment and submerged into the water column (*sub*). To identify an effect of oil droplet binding at the surface, the high concentrations was administered in three ways: like the other treatments, where the eggs were held submerged under the water surface (*H sub*); where the eggs were allowed to float at the surface (*H surf*); and where the eggs were allowed to float and the exposure water was filtered to remove oil microdroplets (water soluble fraction; *H WSF*). WSF fraction was generated as described in (Sørensen et al., 2017).

After exposure, ≈1000 eggs were transferred to recovery flow through tanks with clean water where they were kept until termination of experiment at 3 days post-hatching (dph). Throughout this work, multiple terms are used to define timepoints, based on days post-fertilization (dpf), hours post-exposure start (hpes), and days post-hatching (dph) (Fig. 1A).

2.2. Sampling regime

Duplicate sample collection from all 18 tanks (total of 8 per treatment) for total RNA extraction, body burden and metabolites occurred at 24, 72 hpes and 3 dph for both experiments, as well as 96 and 120 hpes for the *early* exposure. A more thorough time series with triplicate samples (total of 3 per treatment) was collected from a tank of

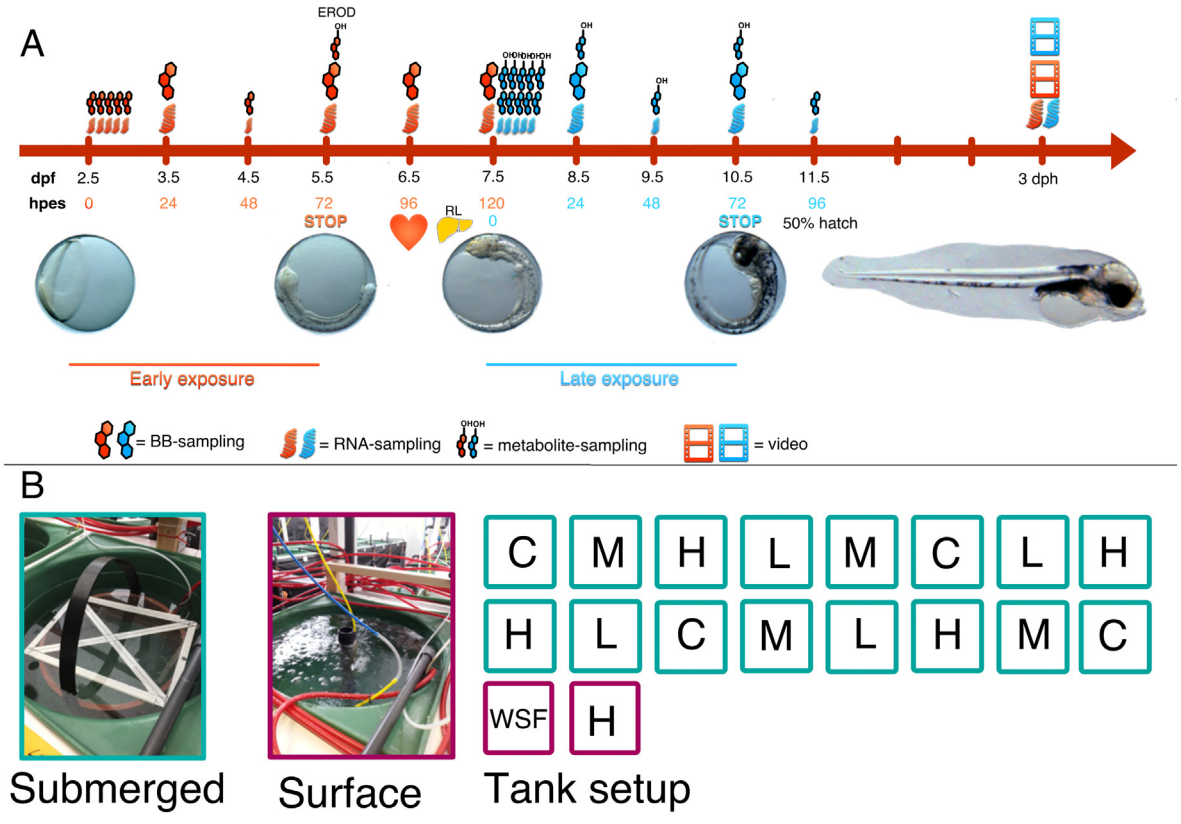

Fig. 1. Experimental design and overview. A) Timeline for experiments in relation to development. Atlantic haddock (*Melanogrammus aeglefinus*) embryos were exposed from 2.5 days post fertilization (dpf) to 5.5 dpf (early exposure) and from 7.5 dpf to 10.5 dpf (late exposure). Heart symbol indicates time point for observation of first heartbeat (6.5 dpf) and liver symbol at the time of sign of rudimentary liver (RL) (approximately 7 dpf) (Hall et al., 2004). Samplings were performed from 1 to 120 h post exposure start (hpes) for the early exposure, and from 1 to 96 hpes for the late exposure. The frequent sampling regime included five sampling points before the 24 h of exposure, and is indicated with multiple sampling symbols. Videos were recorded 3 days post hatching (dph) for both experiments. Red and blue labeling of timepoints and sampling symbols represent early and late exposure, respectively. Small and large sampling symbols indicate sampling of high treatments and control and sampling of all groups, respectively. BB; body burden. B) Tank setup. C = control, L = low treatment, M = medium treatment, H = high treatment, WSF = filtered oil dispersion (water soluble fraction). The turquoise tanks were submerged.

each of four selected treatments (*C*, *H sub*, *H surf* and *H WSF*) following the sampling regime described in Fig. 1A, with sampling points at 1, 2, 4, 8, 12, 24, 48, 72, 96 and 120 hpes. Fewer replicates were taken for *H surf* and *H WSF* at some of the latest time points due to high mortality. The precise number of eggs in each sample pool was counted from microscope pictures, and the range of wet weight of the composite samples was 0.109 g to 0.454 g. The eggs hatched at 11.5 dpf (50% hatch). Therefore, pools of animals from 96 and 120 hpes in the *late* exposure only consisted of larvae.

2.3. Analytical chemistry

2.3.1. PAH analysis in exposure water and body burden samples

Water samples (1 L) were taken from each exposure tank at the beginning and the end of each experiment, preserved by acidification (HCl, pH < 2) and then stored at 4 °C in the dark until further handling. Details are given in Sørensen et al. (2017). In short, the water samples were extracted twice by partitioning to dichloromethane (30 mL) in a separatory funnel (2 min). Deuterated internal standards (naphthalene-d8, biphenyl-d8, acenaphthylene-d8, anthracene-d10, pyrene-d10, perylene-d12 and indeno[1,2,3-c,d]perylene-d12) were added prior to extraction to account for analyte loss during extraction. The combined extracts were concentrated by solvent evaporation prior to analysis by GC–MS. The list of measured 2–5 ring PAH compounds and their alkylated homologues are provided in Supplemental Information.

Samples for PAH body burden were collected frequently (Fig. 1A) to detect immediate changes in PAH uptake. The 48 hpes time point for the *late* exposure was compromised during analysis and data were not available. Each sample collected consisted of 50–100 pooled animals. The eggs were rinsed several times in clean sea water before preserved by flash-freezing in liquid nitrogen and stored at −80 °C. Despite the rinse process some residues of oil were likely to remain on the eggshell and be included in the extraction process as shown in Sørensen et al. (2017).Tissue samples were extracted by solid-liquid extraction and cleaned-up by solid phase extraction (SPE) prior to analysis, as described in detail in Sørensen et al. (2017).

Water and body burden samples were analyzed on an Agilent 7890 gas chromatograph coupled to an Agilent 7010c triple quadrupole mass detector (GC–MS/MS) as described previously in Sørensen et al. (2017). For the body burden samples, a matrix-matched calibration was used, made from the blank extraction of haddock and cod eggs. All glassware for PAH analysis was heated to 450 °C overnight prior to use.

2.3.2. Phenanthrene metabolite analysis in haddock eggs

There are today no analytical methods that are able to detect the whole metabolome of PAH in fish (Beyer et al., 2010). In the present study we have included detection of non-alkylated phenanthrene metabolites as representatives of complex PAH metabolism. The main products of phenanthrene metabolism in fish are dihydroxylated-phenanthrene and monohydroxylated-phenanthrenes (Goksoyr et al., 1987; Pampanin et al., 2016; Pangrekar et al., 2003; Sette et al., 2013). The following standards of target compounds were purchased from Chiron AS (Trondheim, Norway): 1-hydroxyphenanthrene (1-OH-PHE), 2-hydroxyphenanthrene (2-OH-PHE), 3-hydroxyphenanthrene (3-OH-PHE), 4-hydroxyphenanthrene (4-OH-PHE), 9-hydroxy-phenan-threne (9-OH-PHE), *trans*-9,10-dihydroxy-9,10-dihydrophenanthrene (9,10-diol-PHE) and surrogate standard 2-hydroxynaphthalene-d7 (2-OH-NPH-d7). The standard *trans*-1,2-dihydroxy-1,2-dihydrophenanthrene (1,2-diol-PHE) was purchased from MRI Global Carcinogen Repository (Kansas City, MO, USA). Samples for metabolite analysis were collected at 1 timepoint (72 hpes) in *early* exposure and at 8 timepoints (1–72 hpes) in *late* exposure (Fig. 1A), flash frozen and kept at −80 °C until analysis. Details are provided in Supplemental Information for methods of extraction, clean-up and instrumental analysis, using a Waters Acquity high performance liquid chromatograph (LC) coupled with an AB Sciex QTRAP 5500 tandem mass spectrometer (MS).

Sum OHPHEs (ΣOHPHEs) is the sum concentrations of 1-OH-PHE, 2-OH-PHE + 3-OH-PHE (estimate concentration, as these are chromatographically co-eluting isomers), 4-OH-PHE and 9-OH-PHE. Sum PHE-diols (ΣOHPHEs) is the sum concentration of 1,2-diol-PHE and 9,10-diol-PHE. Sum PHE metabolites (Σ PHE metabolites) is the sum concentration of all metabolites measured. The quantitative results were converted from ng metabolites/embryo to ng/g by using average mass of one haddock embryo in egg stage (0.00218 g, calculated from 50 samples each containing over 100 eggs; SD = 0.00018 g). Detection limits for the analytes ranged between 0.015 and 0.9 ng/g wet weight.

2.4. Detection of CYP1A activity

Ethoxyresorufin-O-deethylase (EROD) assay was applied to detect CYP1A activity in the *early* exposure. Activity was measured at the exposure termination at 72 hpes (5.5 dpf). The procedure was performed as described in Gonzalez-Doncel et al. (2011). Briefly, 7-ethoxyresorufin (7ER) was added to live embryos and the CYP1A-catalyzed fluorescing product, resorufin, was detected with fluorescence microscopy. A stock of 7ER (48 mg 7ER/L) (Sigma-Aldrich, Germany) was made in 100% DMSO (Thermo Fisher Scientific). Control, DMSO and crude oil exposed embryos were transferred to 24-well plates where they were incubated in the dark for 1 h in 20 μg 7ER/L or DMSO in sterile sea water. After exposure the solution was drained off and exchanged with sterile sea water. Images of 12–20 embryos per treatment were captured with a digital camera (SPOT Insight 5 Mpx) coupled to a Nikon AZ100 fluorescence microscope. For each set of embryos, two fluorescence images were captured using the rhodamine filter (Ex 545/25 nm and Em 605/70 nm) to detect EROD activity and DAPI filter (Ex 350/50 nm and Em 460/50 nm) to detect the internal fluorescence of high molecular weight PAH compounds. In addition, a corresponding brightfield image was captured for each set of fluorescence. Exposure time was set to 300 ms, and gain was set to 4 for all fluorescence images. Semi-quantitative measurements of EROD fluorescence in the embryos was estimated using the adjusted light intensity in the whole egg in the various treatments. Adjusted light intensity was measured using ImageJ software (http://imagej.nih.gov/ij/) and was calculated using the following formula: Adjusted light intensity = (light intensity in Treatment with 7ER)/(light intensity in Treatment with DMSO).

2.5. Imaging of live embryos/larvae and measurements of cardiac function

Images were taken at all sampling points to define developmental stage, morphological abnormalities and degree of oil droplet accumulation. At 3 dph, all treatments were imaged to assess morphological and cardiac functional endpoints. Images were collected for all exposure tanks in both *early* and *late* exposures. Digital still micro-images and 20-second videos of live 3 dph larvae were obtained using an Olympus SZX-10 Stereo microscope equipped with a 1.2 megapixel resolution video camera (Unibrain Fire-I 785c) controlled by BTV Pro 5.4.1 software (www.bensoftware.com). Image calculations were calibrated with a stage micrometer.

Animals were immobilized in a glass petri dish filled with 3% Methylcellulose (Sigma-Aldrich, Germany) in seawater and kept at 8 °C using a temperature-controlled microscope stage (Brook Industries Inc., Lake Villa, IL, USA). Length of larvae (using segmented line), ethmoid plate, systolic and diastolic diameter of ventricle and atrium and area of edema were measured using ImageJ (http://imagej.nih.gov/ij/) with the ObjectJ plugin (https://sils.fnwi.uva.nl/bcb/objectj/index.html) from images as described previously (Sørhus et al., 2016b). Additionally, eye diameter was quantified, and eye shape and deformities were described according to categories: normal shape (no), bend shape

(be), irregular shape (irr), protruding lens (pl). Six distinct craniofacial phenotypes were identified. Degree of looping of heart was also described (normal looping (n), poor looping (p) and severely poor looping (sp)). The area occupied by edema fluid was quantified as the difference between the total area of the yolk sac and the area of the yolk mass, expressed as a percentage of total yolk sac area. Similarly, ventricular and atrial diastolic (D) and systolic diameter (S) were used to estimate the fractional shortening (FS = (D − S) / D). Measurements from both images and videos were performed blind.

2.6. Oil induced gene expression changes

All animals collected for RNA extraction were frozen in liquid nitrogen and stored at −80 °C after being imaged (as described in the previous section). Total RNA was extracted from frozen pools with 10 eggs/larvae with Maxwell HT simplyRNA (Promega Corporation) according to the manufacturer's instructions using Biomek 4000 Automated liquid handler (Beckman coulter). Quantity and quality of the extracted total RNA was checked using Nanodrop spectrophotometer (NanoDrop Technologies, Wilmington, DE, USA) and Bioanalyzer (Agilent Technologies, Santa Clara, CA, USA) respectively. All samples included had RNA integrity number above 8, and A260/230 and A260/280 above 1.8. Complementary DNA (cDNA) was subsequently generated using SuperScript VILO cDNA Synthesis Kit (Life Technologies Corporation), according to the manufacturer's instructions, and was normalized to obtain a concentration of 50 ng/μL. The described frequent sampling regime was followed to detect immediate gene expression changes (Fig. 1A and see the previous "Section 2.2 Sampling regime").

Specific primers and probes for real-time qPCR analysis of Atlantic haddock were designed with Primer Express software (Applied Biosystems, Carlsbad, California, USA) (*cyp1a* and the technical reference Elongation factor 1 alpha (*ef1a*)) or Integrated DNA Technology (IDT) probe and primer design software (IDT Inc., Iowa, USA) (*cyp1b, cyp1c, cyp1d, abcb1, rhag* and technical reference Retinoic acid receptor RXR beta A (*rxrba*)), according to the manufacturer's guidelines. Primer and probe sequences are given in Supplementary Table S1. Detailed protocol for Real-time qpcr assays and analysis can be found in Supplementary Information.

2.7. Localization of rhag gene expression

Localization of *rhag* gene expression in early life stages of haddock is unknown. Therefore, *in situ* expression of *rhag* was examined using a method derived from previous whole mount *in situ* protocols (Hall et al., 2003; Thisse and Thisse, 2008; Valen et al., 2016). Dechorionating haddock embryos smaller than 10 dpf is very challenging. We therefore performed whole mount *in situ* hybridization on unexposed 10 dpf embryos to determine location of *rhag* in early life stages of fish. Detailed protocol can be found in Supplementary Information.

2.8. Statistics

Statistical differences in CYP1A activity, morphology, cardiac function, PAH concentration in the water, PAH body burden, and OHPAH metabolites were tested using one-way ANOVA with Dunnet's multiple comparison in R (The R Foundation for Statistical Computing Platform) after testing for normality using Shapiro-Wilk test in R. In the gene expression data, statistically significant differences were tested using both one-way and two-way ANOVA with Dunnet's multiple comparison in R after testing for normality. PAH concentration in water and tissue, OH-PAH metabolites and gene expression data were log-transformed before statistical testing due to large differences in concentrations and thus standard deviation. In craniofacial and eye phenotypes, appearance of silent ventricle and cardiac looping, statistical differences between treatments and control were evaluated using chi-square test. Statistical difference was denoted $p < 0.05$ (*), $p < 0.01$ (**), and $p < 0.001$ (***). Error bars in all figures represent the standard deviation of the mean.

2.9. Ethics statement

The animals were monitored daily, and any dead larvae were removed. All sampled embryos and yolk sac larvae were euthanized immediately in liquid nitrogen. The Austevoll Aquaculture Research station has the following permission for catch and maintenance of adult Atlantic haddock: H-AV 77, H-AV 78 and H-AV 79. These are permits given by the Norwegian Directorate of Fisheries. Furthermore, the Austevoll Aquaculture Research station has a permit to run as a Research Animal facility using fish (all developmental stages), with code 93 from the national Institutional Animal Care and Use Committee; National Animal Rights Association, although no approval is necessary to perform studies with fish embryos and yolk sac larvae.

3. Results

Overall, both *early* and *late* exposure resulted in functional and morphological abnormalities, but they were more severe in the *early* exposure (Figs. 2, 6 and Tables 2 and 3). Tissue uptake of PAHs was higher in the *early* exposure, followed by a stronger, but delayed *cyp1a* induction (Figs. 3, 4 and 5). The *H WSF* treatment showed very few oil induced abnormalities in both exposures. Gene expression patterns were unique between *early* vs *late* exposures (Figs. 5, 7, S7 and S8).

3.1. Oil droplet fouling in surface and submerged embryos

Oil droplet fouling was observed on embryos in both submerged (*L, M, H sub*) and surface (*H surf*) exposures regardless of timing, and was evident after only 1 h of exposure (Fig. 2A and B, top panels). The oil droplet fouling effect was higher in the surface (*H surf*) exposure due to the accumulation of oil microdroplets on the surface (Fig. 2). While oil droplets in the *early* exposure were distributed all over the surface, the *late* exposure embryos mainly accumulated oil droplets at one area on the chorion (Fig. 2B, filled black arrows). In the filtered high treatment (*H WSF*), no oil droplets were detected on the chorion (Fig. 2A and B, right panel). After transfer to clean water, some of the droplets appeared to be washed off. However, in addition to a reduced number of apparent oil droplets (brown), translucent droplets were now visible on the surface (white arrow head Supplementary Fig. S1). This phenomenon was not observed in the *late* exposure due to hatching that occurred shortly after end of exposure (11.5 dpf) (Fig. 1).

3.2. Oil exposure and PAH uptake

3.2.1. PAH concentration in water and tissue

We successfully delivered concentrations of dispersed crude oil to the exposure tanks during the experiments. Total PAHs (dissolved and droplet associated) were monitored at the beginning and end of each exposure experiment (Fig. S2). The PAH concentration in water was lower in the *H WSF* than the other high treatment, because *H WSF* did not include PAH contribution from the oil droplets. There were some differences in the total PAH concentration between the two experiments, but there were clear gradients among the different treatment in both studies (Table 1).

An immediate and prominent uptake of PAHs into the embryo was detected (Fig. 3). Body burden measurements of all treatments at all time-points in both experiments had statistically significant elevated concentrations of PAH compared to control. Average total PAH concentrations in tissue in the exposed treatments for *early* exposure ranged from 38 (1 hpes, *H WSF*) to as high as 7800 ng/g ww (72 hpes, *H surf*). Values in the *late* exposure were between 75 (24 hpes, *L*) and 3000 ng/g ww (72 hpes, *H surf*). Notably, despite higher PAH concentrations in water in the *late* exposure, the highest concentrations in the

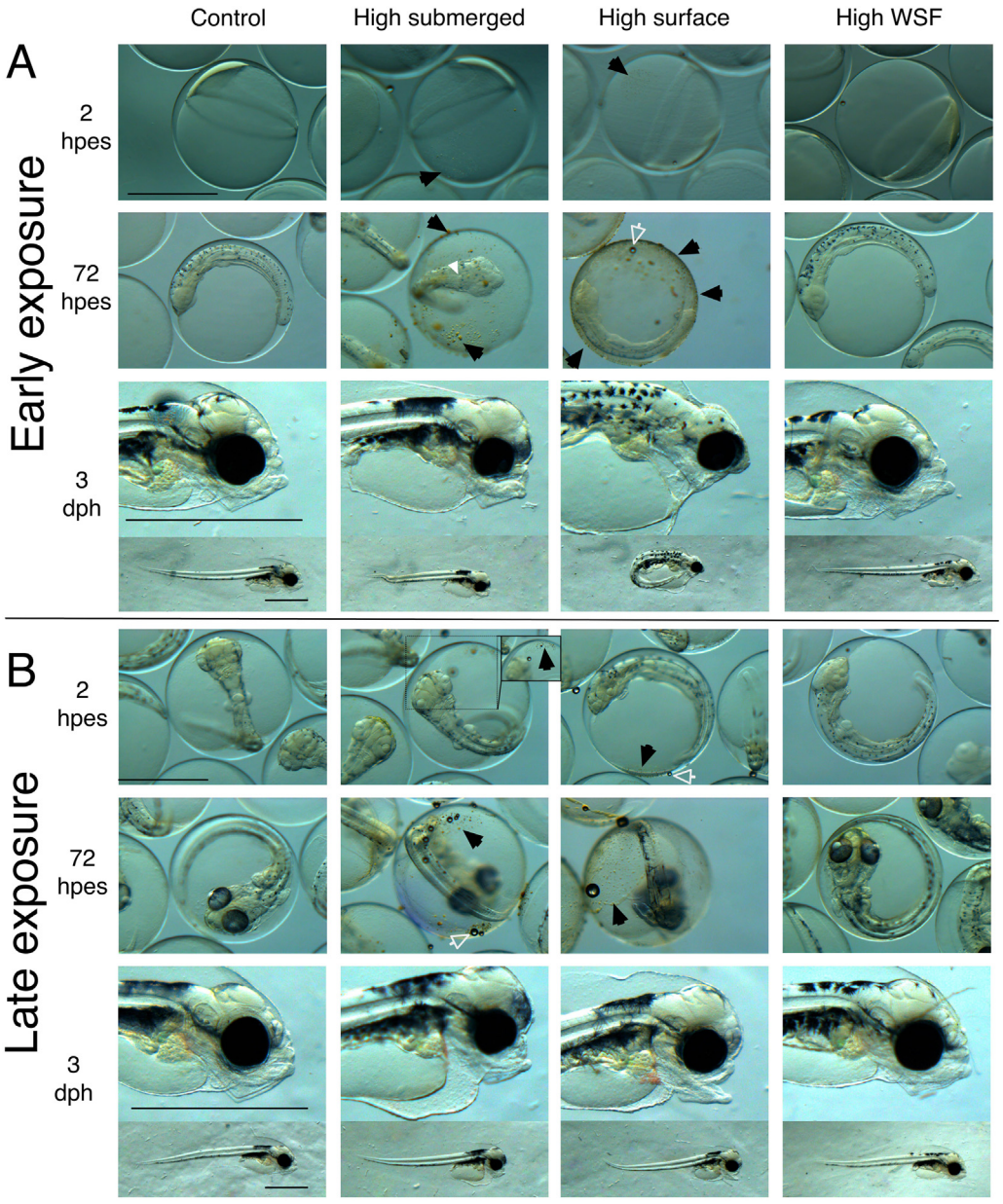

Fig. 2. Oil droplet fouling and morphology. A) early and B) late embryonic exposure of Atlantic haddock. Top panels show 2 h post exposure start (hpes), middle panels 72 hpes (termination of exposure) and lower panels display representative phenotypes at 3 days post hatching (dph). Black arrows: oil droplets. White arrow head: indicates cardiac cone. White open arrow: air bubble trapped on the chorion. WSF: water soluble fraction. Scale bar: 1000 μm.

tissue were found in the *early* exposure. The concentrations in the *H WSF* treatments (in which the water was filtered) were more similar to the medium treatment, despite sharing the same oil content of the high treatment (300 μg oil/L) (Fig. 3A). Fig. 3B shows the profile of PAHs at 72 hpes. Notably, the high molecular weight (HMW) PAH treatment (inset in Fig. 3B) found in medium, *H sub* and *H surf* treatments, was lacking in the *H WSF* treatment. These HMW PAHs, e.g. PYRs and CHRs, accumulated substantially more in the *H surf* than in other treatments. In addition, in the *H surf*, the concentrations of these HMW PAHs were up to four times higher in *early* vs *late* exposure (Fig. S3). Detailed profiles for individual PAHs at each time point are documented in Supplementary Dataset S1.

3.2.2. Hydroxylated phenanthrene metabolites

Hydroxylated phenanthrene metabolites were analyzed in the control and three high treatment groups (*H sub*, *H surf* and *H WSF*) at *early* (only at termination of exposure, 72 hpes) and *late* exposure (1–72 hpes). Metabolites assessed are presented as sum of monohydroxyphenanthrenes (ΣOHPHE) and sum of dihydrodiol phenanthrenes (ΣPHE-diols) (Fig. 4). Within these groups 1,2-diol-PHE was the dominating metabolite and accounted for approximately 90% of total detected metabolites (average of all treatments). Of the ΣOHPHE, 1-OH-PHE was the most abundant and contributed with 9% of the total metabolites (Supplementary Dataset S2).

Metabolite concentrations at termination of exposure (72 hpes) for *early* exposure were approximately 3 times lower than *late* exposure (Fig. 4A). In the *late* exposure, where we analyzed for a metabolite profile over time, we observed significant concentrations of phenanthrene metabolites in all high treatment groups after 24 hpes, and these concentrations continued to increase until termination of exposure (Fig. 4B). The maximum body burden of PHE metabolites was found in the *H surf* treatment (72 hpes) in a concentration of

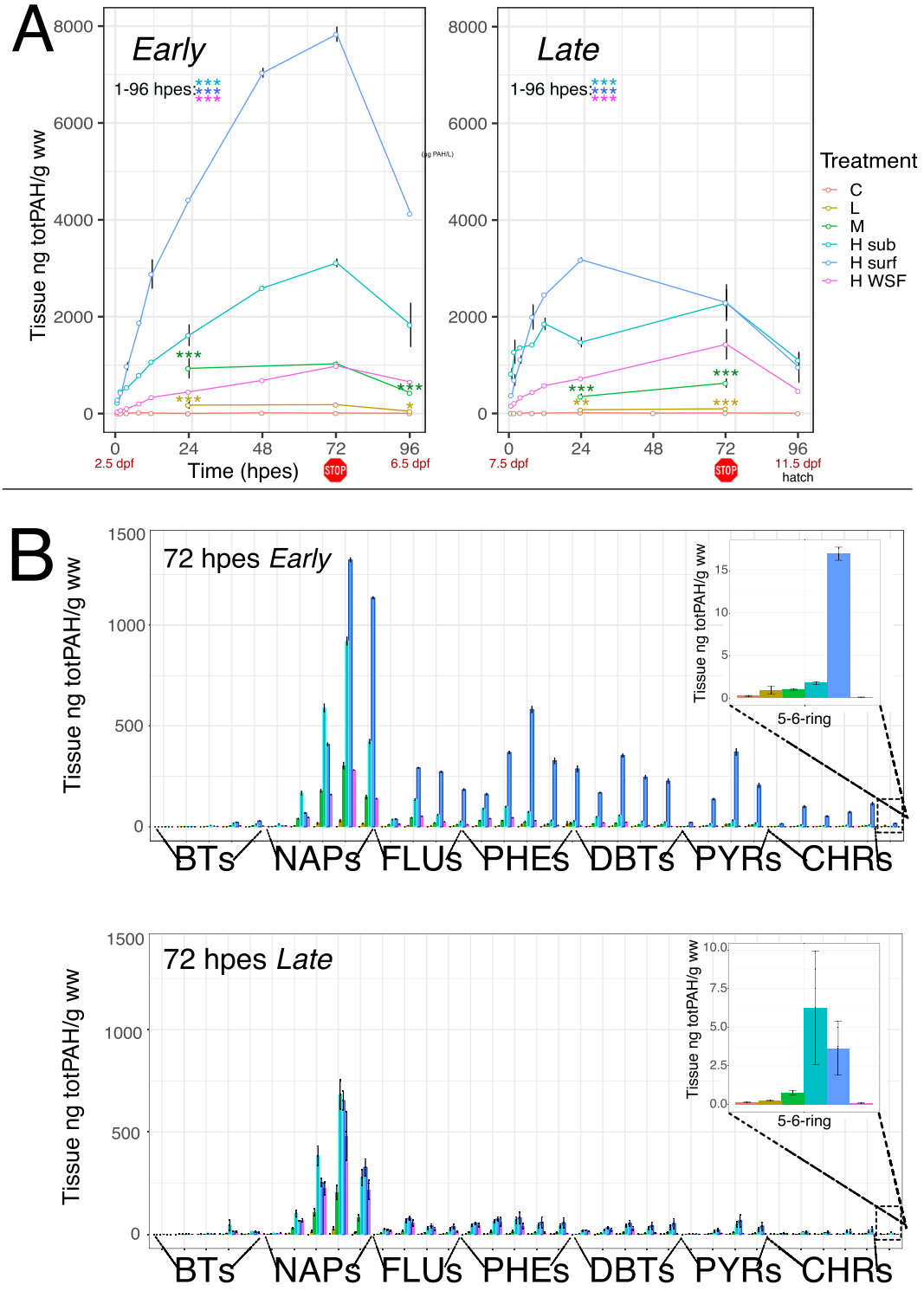

Fig. 3. Tissue uptake of PAHs. A) Total body burden of PAHs from 1 to 96 h post exposure start (hpes) in early (left panel) and late (right panel) exposure. Termination of exposure was after 72 h. Statistical difference from control was tested at each time point with one-way ANOVA and significant differences are indicated by **: $p < 0.01$ and ***: $p < 0.001$. Note, at 96 hpes only one replicate from H surf and H WSF (early exposure) and H WSF (late exposure) was analyzed. B) PAH profile at termination of exposure (72 hpes) in early (left panel) and late (right panel) exposure. Inset: magnification of sum of 5–6 ring distribution in the treatments. Error bars represent ±standard deviation. dpf: days post exposure, C: control, L: low treatment, M: medium treatment, H sub: high treatment submerged, H surf: high treatment surface, H WSF: high treatment water soluble fraction, BTs: sum of benzothiophenes, NAPs: sum of naphthalenes, FLUs: sum of fluorenes, PHEs: sum of phenanthrenes, DBTs: sum of dibenzothiophenes, PYRs: sum of pyrenes, CHRs: sum of chrysenes.

45 ng/g ww. This is in the similar concentration ranges as the body burden of the parent PHE (95 ng/g ww found after 24 hpes). The metabolites in the *H WSF* were approximately 1/3 that of *H sub*, although they followed a similar trend over time. (Fig. 4B). The correlation between phenanthrene metabolites and body burden (Fig. 4C) demonstrated that the rate of biotransformation exceeded the rate of PAH uptake. By 12 hpes (*H sub*) and 24 hpes (*H surf*), the curve turned back on itself indicating that the formation of metabolites was increasing while the PAH body burden had begun to decrease (even under continuous exposure).

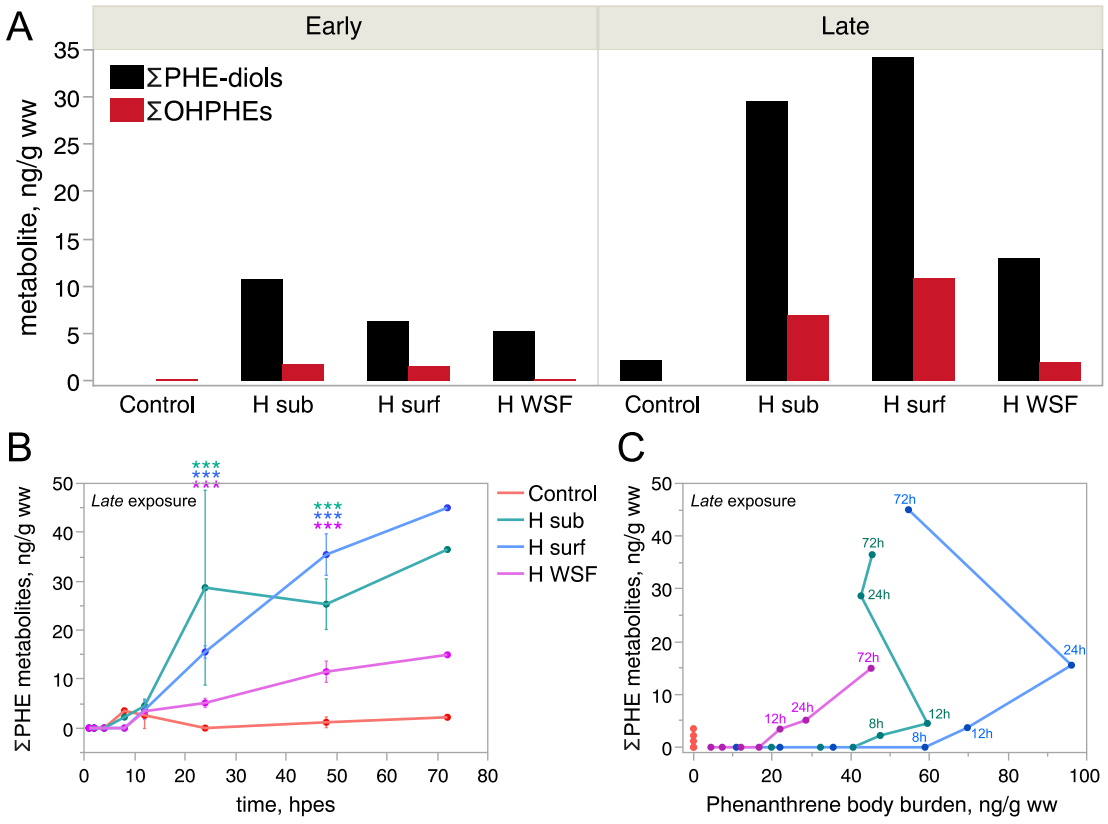

Fig. 4. Concentration of phenanthrene metabolites in tissue. A) Concentrations of PHE-diols and OHPHEs at 72 hpes in early and late exposures (one sample per treatment). B) Concentrations of ΣPHE metabolites over time in late exposure. Statistical difference from control was tested at 12 hpes, 24 hpes and 48 hpes with one-way ANOVA with Dunnet's multiple comparison, and significant differences are indicated by ***: $p < 0.001$. C) Sum of phenanthrene metabolites versus mean body burden of phenanthrene in late exposure. Error bars represent ±standard deviation. H sub: high treatment submerged, H surf: high treatment surface, H WSF: high treatment WSF.

3.3. Temporal expression of cyp1a, cyp1b, cyp1c and cyp1d and EROD activity

3.3.1. Temporal expression of cyp1s

Expression of *cyp1a* was immediate in both experiments. It was increasing throughout the *early* exposure (Fig. 5A), and the expression stayed steady from 12 to 72 hpes at the late exposure (Fig. 5B). In the *early* exposure a 5- and 6-fold significant change of *cyp1a* was detected after 8 h of exposure in *H sub* and *H surf*, respectively (Fig. 5A). All treatments at investigated time-points were up-regulated from 12 hpes (Fig. 5A). In the *late* exposure, the induction of *cyp1a* was much more rapid with 2 fold up-regulation after only 2 h of exposure in the *H surf* treatment (Fig. 5B). From 8 hpes and onward significant up-regulation of *cyp1a* was seen in all treatment groups including low and medium at 24 and 72 hpes (Fig. 5B).

Induction of *cyp1a* correlated with tissue uptake of PAH (Fig. S4). However, one of the low treatment tanks, L4, showed low PAH uptake and *cyp1a* induction in both *early* and *late* exposures. It was therefore considered an outlier and eliminated for further analysis in both experiments. Embryos from the L4 tank clustered to the control tanks rather than the low treatment tanks at both 24 hpes and 72 hpes (Fig. S5, 72 hpes).

The expression of the other *cyp1* paralogs, *cyp1b* and *cyp1c*, was delayed in the *early* exposure and generally followed the same pattern as *cyp1a* expression in the *late* exposure (Fig. 5). The expression profile over time for the control treatment showed a highly dynamic temporal expression of *cyp1b*, *cyp1c* and *cyp1d*. Expression of *cyp1a*, on the other hand showed a stable expression throughout embryonic development (Fig. S6A–D). In the early exposure, *cyp1c* was not appreciably expressed regardless of treatment until 48 hpes (Fig. 5C), and at 72 hpes a 200 fold up-regulation related to development (independent of oil exposure) was observed in the control group (Fig. S6C). Similarly, a general up-regulation of *cyp1b* was seen from 24 hpes in all treatments including control (Fig. S6B). A significantly different upregulation in surface treatment was observed at the two latest time points (Fig. 5C). For *cyp1d*, no transcripts were detected at any of the time points in either treatment/control in the *early* exposure. In the *late* exposure, a general increased expression of *cyp1d* was seen at 72 hpes (Fig. S7). At 9 days since exposure termination (*early* exposure) at 3 dph one of the treatments *H surf*, still had significant up-regulation of one of the *cyp1*s, namely *cyp1b* (Fig. S8A–D, left panel). At 3 dph after 4 days of recovery (*late* exposure), significant up-regulation of several *cyp1*s was observed in *H surf* and in *H sub* treatments (Fig. S8A–D, right panels).

3.3.2. CYP1A activity

An EROD assay was applied to detect CYP1A activity and was measured at 72 hpes (5.5 dpf) in the *early* exposure. CYP1A activity was detected in the skin, mainly in the trunk, and in the otoliths in the *H sub* and *H surf* exposures. Animals in the low and medium treatments showed EROD activity in the trunk, while very little activity was detected in *H WSF* (Fig. S9). No specific fluorescence was detected in the embryos incubated in clean sea water (Fig. S9) or sea water with DMSO (images not shown). The internal fluorescence activity of the high molecular weight PAHs in the oil droplets are shown in Fig. S9C.

3.4. Crude oil induced malformations

Craniofacial, eye and growth abnormalities were seen in both exposures at 3 dph (Table 2). We defined six distinct concentration-

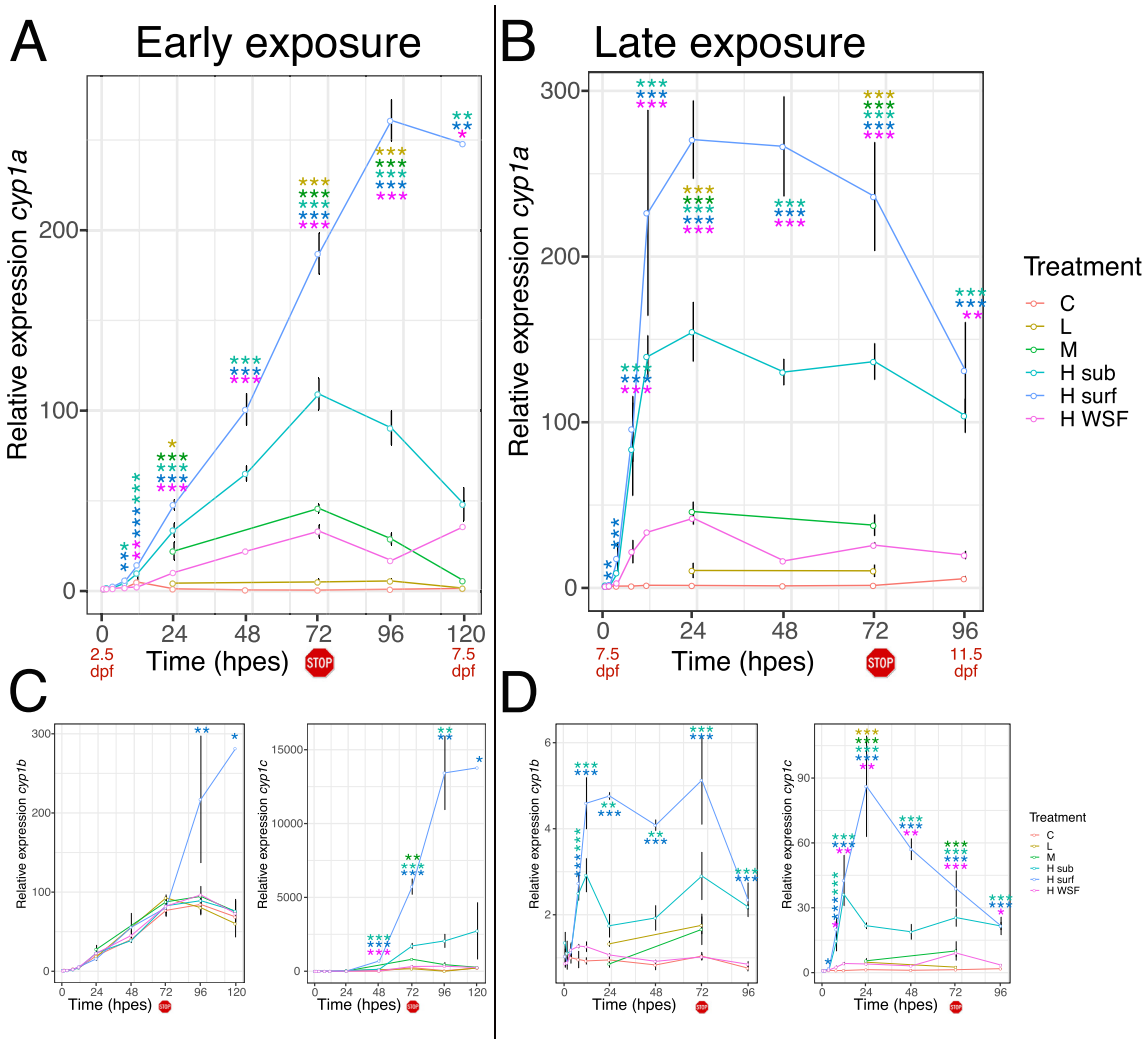

Fig. 5. Relative expression of cyp1s. Relative expression of cyp1a after early (A) and late (B) exposure. C) shows relative expression of cyp1b (left panel) and cyp1c (right panel) after early exposure, while D) displays cyp1b (left panel) and cyp1c (right panel) after late exposure. Expression was related to control treatment at exposure start to detect both developmental and treatment related expression. Termination of exposure is indicated with a stop icon. Statistical difference from control at each time point was tested with one-way ANOVA with Dunnet's multiple comparisons and significant differences are indicated by *: $p < 0.05$, **: $p < 0.01$ or ***: $p < 0.001$. At 120 hpes in the early exposure, only one sample was collected for H surf and H WSF. Error bars represent ±standard deviation. Note: The ranges of the y-axes are not the same for the various panels. hpes: hours post exposure start, dpf: days post exposure, C: control, L: low treatment, M: medium treatment, H sub: high treatment submerged, H surf: high treatment surface, H WSF: high treatment WSF.

dependent craniofacial phenotypes, given here in increasing severity: Phenotype 1 (PT1) and phenotype 2 (PT2) with reduced upper jaw, phenotype 3 (PT3) with a posteriorly twisted upper jaw, phenotype 4 (PT4) with posteriorly twisted jaws in general, phenotype 5 (PT5) with an underdeveloped upper jaw and hanging lower jaw and phenotype 6 (PT6) with severe reduction of all jaw structures with reduced brain structures, abnormal finfold, spinal curvature and poor dorsal rotation of the head (Fig. 6).

The most severe craniofacial malformations were observed after early exposure (Fig. 6A, lower panel, Table 2). In the *late* exposure, the craniofacial malformations were generally milder, and the difference between the *H sub* and *H surf* treatments were less evident (Fig. 6). Along with craniofacial phenotype, the ethmoid plate was significantly reduced in the *H sub* and *H surf* treatments (Table 2). Total length of the larvae was reduced in all exposed treatments (Table 2).

Eye shape and diameter were affected by oil exposure at both time points. Four eye phenotypes were observed: normal round shape (no), bend shape (be), irregular shape (irr) and protruding lens (pl) (Table 2). The frequency of any eye phenotype was higher in the *early* exposed animals, and the most severe phenotype, protruding lens, was only found in *H sub* (8%) and *H surf* (12%) treatments. No effect on eye shape was seen in *H WSF* regardless of timing of exposure (Table 2). Severe reduction in eye diameter was found in the *early* exposed *H surf* and *H sub* animals (Table 2). Less effect on eye size was observed in the *late* exposure, only medium treatment showed significantly reduced eye diameter.

Table 1
Average concentrations of total PAHs in water. C; Control, L; Low concentration, M; Medium concentration; H sub; High concentration submerged, H surf; High concentration surface, H WSF; High concentration water soluble fraction, SD; standard deviation.

Treatment	*Early* exposure		*Late* exposure	
	Average (µg PAH/L)	SD (+/−)	Average (µg PAH/L)	SD (+/−)
Control	0.04	0.01	0.04	0.01
Low	0.47	0.61	0.5	0.2
Medium	2.3	2.4	2.2	0.8
H sub	5.2	1.7	9.7	2.7
H surf	6.4	0.8	8.3	2.9
H WSF	3.7	1.0	6.3	0.9

Table 2
Morphological abnormalities after early and late embryonic exposure. WSF; water soluble fraction, SD; standard deviation, N; total number of animals analyzed, No; normal phenotype, PT; phenotype, no; normal eye shape be; bend eye shape, irr; irregular eye shape, pl; protruding lens, nlo; normal looping, plo; poor looping, splo; severely poor looping. Statistical significant difference from control is indicated by asterisks.

		Total length mm		Ethmoid plate µm		Eye diameter µm		Craniofacial phenotype							Eye phenotype				Cardiac looping			
		Average ± SD	N	Average ± SD	N	Average ± SD	N	No	MBD	BD	UJB	TJB	DV	HB	no	be	irr	pl	nlo	plo	splo	*p* value
Early exposure 3 dph	Control	4.8 ± 0.3	59	170 ± 28	51	175 ± 17	52	95	0	0	5	0	0	0	94	4	2	0	93	7	0	
	Low dose	4.8 ± 0.4	47	162 ± 24	47	184 ± 13	47	77	2	4	17	0	0	0	90	0	9	0	76	24	0	0.0054**
	Medium dose	4.7 ± 0.3	61	174 ± 19	61	177 ± 12	59	72	0	0	28	0	0	0	82	8	10	0	60	40	0	<0.00001***
	High submerged	4.6 ± 0.4***	60	147 ± 19***	61	167 ± 16***	60	42	11	9	30	5	4	0	78	4	10	8	31	57	11	<0.00001***
	High surface	3.5 ± 0.4***	18	47 ± 37***	19	131 ± 9***	20	0	0	0	0	0	47	53	68	4	16	12	0	0	100	<0.00001***
	High WSF	4.8 ± 0.3	20	164 ± 24	20	187 ± 13	20	100	0	0	0	0	0	0	100	0	0	0	95	5	0	0.86
Late exposure 3 dph	Control	4.7 ± 0.2	75	156 ± 21	79	177 ± 9	78	96	4	0	0	0	0	0	100	0	0	0	88	12	0	
	Low dose	4.6 ± 0.2*	59	148 ± 17	59	179 ± 9	59	81	17	2	0	0	0	0	98	0	2	0	95	5	0	0.24
	Medium dose	4.6 ± 0.2***	58	154 ± 26	59	173 ± 10*	58	78	13	4	0	4	2	0	95	2	4	0	74	26	0	0.047*
	High submerged	4.5 ± 0.3***	97	124 ± 27***	74	173 ± 11	78	37	32	25	0	4	1	0	72	6	21	1	42	58	0	<0.00001***
	High surface	4.3 ± 0.2***	20	116 ± 19***	20	173 ± 9	19	0	37	53	0	0	11	0	68	5	26	0	20	80	0	<0.00001***
	High WSF	4.5 ± 0.2**	20	149 ± 30	20	183 ± 7	19	85	15	0	0	0	0	0	100	0	0	0	90	10	0	0.91

* $p < 0.05$.
** $p < 0.001$.
*** $p < 0.0001$.

3.5. Cardiac malformations

3.5.1. Morphological abnormalities

The size of the heart was reduced in both exposures, but only *early* exposure resulted in severely malformed hearts with poor looping (Table 3). After *early* exposure, an effect on atrial dimensions was only detected in the *H surf* and *H sub* treatment (Table 3). The ventricular diastolic diameter was reduced in all exposure treatments (9–43%) except for *H WSF*, and the *H surf* treatment also showed reduced ventricular systolic diameter (38%) (Table 3). There was no effect on atrial dimensions after *late* exposure in any of the treatments. However, ventricular systolic and diastolic diameters were reduced in both *H sub* (12% and 19%, respectively) and *H surf* treatments (19% and 31%, respectively) in the *late* exposure (Table 3). The hearts were not as malformed as in the *early* exposure, and no incidences of severely poor looping was observed (Table 3).

3.5.2. Functional abnormalities

In both exposures ventricular contractility (VFS) was reduced (Table 3). Notably, reduced contractility was also evident in the lower treatments in the *early* exposure. In addition, several animals suffered from a non-contracting ventricle, defined as silent ventricle (SiV). In the *early* exposure, we observed a concentration-dependent prevalence of SiV in all treatments with oil droplets. Silent ventricles were most prevalent in the *H surf* treatment (73%) with the severely abnormally shaped hearts. The only treatment in *early* exposure with no incidence of SiV was *H WSF*. In the *late* exposure, there were fewer SiVs in all treatments; however, we still observed SiV in 60% of the *H surf* animals, even though their heart morphology was normal compared to the *early* exposed animals. Reduced heart rate (bradycardia) was only observed in the *H surf* treatment at the *early* exposure, while increased heart rate (tachycardia) was seen in *H WSF* treatment in the *late* exposure (Table 3).

Edema formation, a consequence of circulation abnormalities, was seen in both exposures but in more treatments in the *late* exposure (Table 3). Yolk sac size is dependent on hatching time and rate of yolk consumption. We observed an increased average yolk sac size, indicating a decreased yolk utilization in the *H surf* treatment after *early* exposure. The opposite was observed in the *late* exposure (Table 3).

3.6. Temporal expression of genes in response to early and late oil exposure

Generally, the response in gene expression was different for each gene between the two exposures (Fig. 7). Oil-induced differential expression of *bmp10* was independent of circulation with an immediate trend of up-regulation in the *late* exposure. Expression of *rhag* and *abcb1* were delayed and were subsequent of *cyp1a* expression. Expression dynamics for the control group in all genes are shown in Fig. S6.

Exposure-related up-regulation of *bmp10*, a calcium regulated gene involved in cardiogenesis, was observed before first heart beat at the cardiac cone stage (72 hpes, 2.4 fold in *H surf* treatment) (Fig. 7). From exposure start to 24 hpes no expression of the potent signaling molecule, was detected at the mRNA concentration in any of the treatments including control (Fig. 7A and Fig. S6E). Induction of *bmp10* (~7 fold) was first initiated at 4 dpf (48 hpes) in all treatments including control and showed an increasing expression throughout the measured period (Fig. 7A and Fig. S6E). Significant up-regulation in the *H surf* treatment was observed at 72 and 96 hpes in the *early* exposure (Fig. 7A). At the *late* exposure the expression of *bmp10* was more variable throughout the period. A trend of up-regulation was seen from 4 hpes. In particular, *H sub* and *H surf* treatments were significantly different from control overall in the investigated period (two ANOVA $p < 0.01$) (Fig. 7B). No significant expression changes were detected at 3 dph after either early or late exposure (Fig. S8E).

Significant up-regulation of *abcb1* was seen after *early* exposure but during *late* exposure (Fig. 7). In the *early* exposure, up-regulation was only seen in *H sub* and *H surf* treatments (Fig. 7A). While in the late exposure, up-regulation was observed in medium and all high concentrations (Fig. 7B). No differential expression of *abcb1* was seen at 3 dph after any exposure treatment (Fig. S8H).

Up-regulation of *rhag* was seen in *H sub* and *H surf* treatments at both exposures (Fig. 7). Differential expression of *rhag* was much more rapid in the *late* exposure (after completion of organogenesis), and significant up-regulation was seen in both *H sub* (2–3 fold) and *H surf* (3–4 fold) treatments at 24 hpes and throughout the examined period. No differential expression of *rhag* was detected at 3 dph in either *early* or *late* exposure (Fig. S8G).

3.6.1. Whole mount in situ hybridization of rhag

To determine location of *rhag* in early life stages of haddock, we performed whole mount *in situ* hybridization (WISH) on unexposed

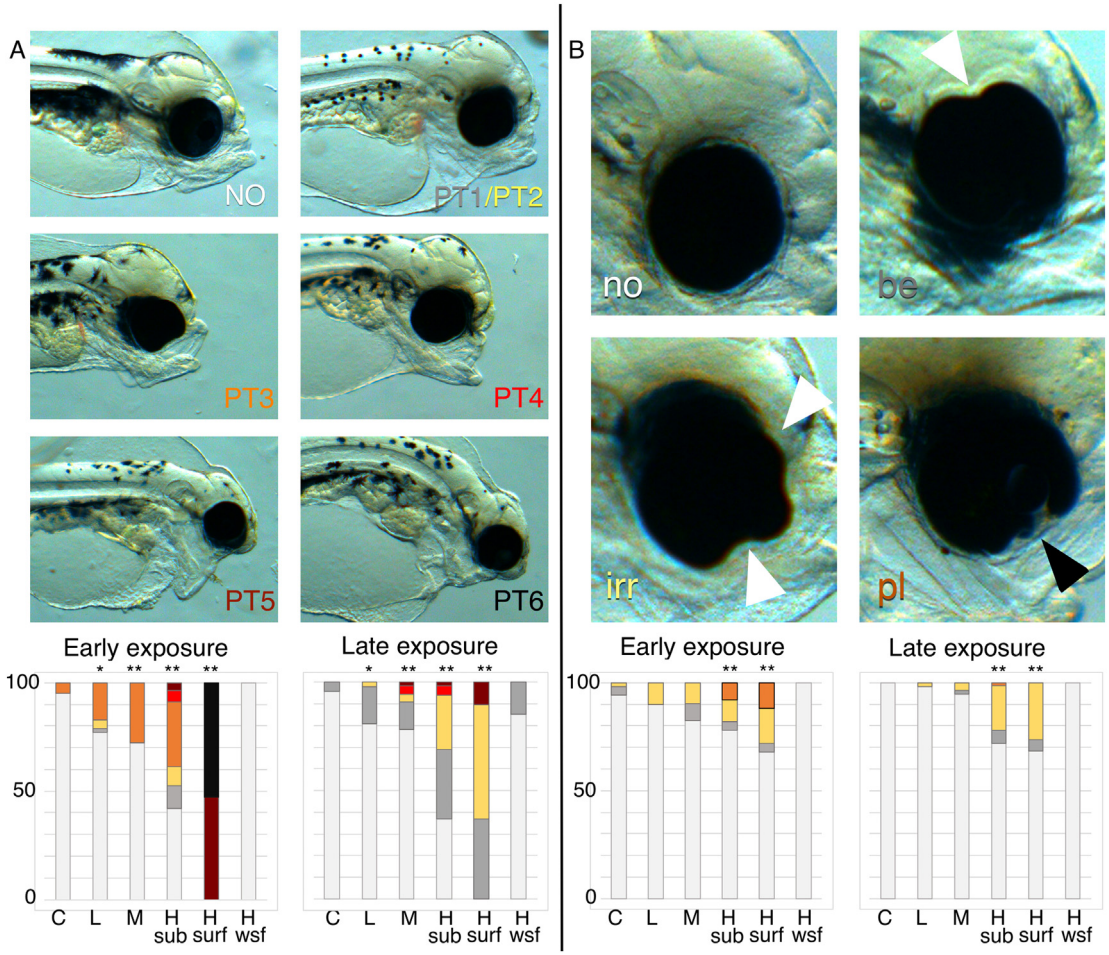

Fig. 6. Oil induced craniofacial and eye phenotypes. A) Oil induced craniofacial phenotypes, NO: normal phenotype, PT1–6; Phenotype 1–6. The bottom panel shows the distribution of the craniofacial phenotypes after early and late exposure at 3 days post hatching. Coloration code: white: NO, grey: PT1, yellow: PT2, orange: PT3, red: PT4, dark red: PT5, black: PT6. B) Oil induced eye phenotypes, no: normal eye shape (white), be: bend shape (grey), irr: irregular shape (yellow), pl: protruding lens (orange). Bottom panel shows the distribution of eye phenotypes in early and late exposures. White arrow heads indicate irregularities in the eye shape, and black arrow head indicate protruding lens. Statistical difference from control was tested with Chi-square, and $p < 0.01$ is indicated by **. C: control, L: low treatment, M: medium treatment, H sub: high treatment submerged, H surf: high treatment surface, H WSF: high treatment water soluble fraction, PT: phenotype.

10 dpf embryos (Fig. 8). In unexposed 10 dpf Atlantic haddock embryos, expression of *rhag* was observed in a line following the branchial arch blood vessels (Fig. 8). No expression was found anywhere else in the embryos, however, due to auto staining, the yolk sac was removed prior to coloration, and thus, the syncytial layer and yolk sac were not available for analysis. The technical negative control (sense) showed no coloration (Fig. 8C).

4. Discussion

In this study we aimed to link the consequences of short-term crude oil exposures in two embryonic phases to metabolism and abnormal circulation by investigating morphological and functional phenotypes and related gene expression. In general, the embryotoxic consequences of an oil exposure were more severe in the *early* exposure animals. Severe cardiac and craniofacial abnormalities in the highest treatments exposed to micro oil droplets were highlighted. The large difference in phenotypic outcome in *early* vs *late* exposure could be explained both by the prolonged exposure and less developed response system. First, particularly in the *early* exposure, the treatments exposed to micro oil droplets experienced a prolonged exposure evident by visible oil droplets on the chorion and a prolonged *cyp1a* response. Second, the *early* exposure started prior to or at the time of onset of zygotic transcription (Sørhus et al., 2016a), in which the embryo has a slower transcriptional response. Consequently, we observed a delayed response in gene expression of all genes evaluated, including *cyp1a* which is crucial for the first phase in xenobiotic metabolism (Goksøyr, 1995). Higher oil droplet binding and most likely, accumulation, contributed to a higher body burden of PAHs in the *early* exposure, while the concentrations of PHE metabolites were 2–3 times higher in the *late* exposure.

Exposing embryos at two developmental time points gave us a unique opportunity to phenotypically anchor temporal gene expression changes and continue to unravel underlying mechanisms of crude oil toxicity. Exposure during early cardiac development, and after onset of heartbeat enabled us to evaluate whether the expression response for the various genes were due to direct effect or secondary to abnormal circulation. Furthermore, we linked gene expression to metabolism by investigating expression in context of CYP1A regulation, PAH uptake and appearance of metabolites. Mainly, we suggest that *cyp1a*, *cyp1b*, *cyp1c* and *bmp10* are directly induced by parent compounds in the oil. To illustrate, these genes are expressed in the *late* exposure before metabolites were detected. Subsequently, *abcb1* and *rhag*, which are linked to transport of xenobiotic products (Choudhuri and Klaassen, 2006) and nitrogenous waste (Caner et al., 2015), respectively, showed a delayed response corresponding to energy consumption (Wang et al., 2019) and transport in xenobiotic metabolism (Kimura et al., 2007).

Table 3
Cardiac abnormalities after early and late embryonic exposure. WSF; water soluble fraction, AS; atrial systolic diameter, N; number of animals analyzed, AD; atrial diastolic diameter, VS; ventricular systolic diameter, VD; ventricular diastolic diameter, AFS; atrial fractional shortening, VFS; ventricular fractional shortening, BPM; beats per minute, SiV; Silent ventricle, SD; standard deviation. Statistical significant difference from control is indicated by asterisks.

		AS μm		AD μm		VS μm		VD μm		AFS %		VFS %		Edema %		Yolk sac mm^2		BPM		SiV %	
		Average ± SD	N	Average ± SD	N	Average ± SD	N	Average ± SD	N	Average ± SD	N	Average ± SD	N	Average ± SD	N	Average ± SD	N	Average ± SD	N	%	N
Early exposure 3 dph	Control	101 ± 14	42	122 ± 18	42	90 ± 14	54	106 ± 20	54	18 ± 7	42	14 ± 7	54	15 ± 8	61	0.21 ± 0.08	61	93 ± 9	61	2	54
	Low dose	94 ± 15	20	115 ± 18	20	86 ± 9	34	96 ± 13*	34	18 ± 8	20	10 ± 7*	32	12 ± 6	48	0.24 ± 0.10	48	90 ± 7	38	13**	48
	Medium dose	94 ± 14	22	114 ± 17	22	85 ± 14	50	94 ± 15**	50	20 ± 9	22	9 ± 8**	50	13 ± 9	61	0.24 ± 0.11	61	89 ± 10	53	24***	51
	High submerged	92 ± 18*	42	115 ± 20***	44	84 ± 16	57	92 ± 20***	57	20 ± 9	42	8 ± 9***	57	17.6 ± 11	61	0.24 ± 0.11	61	91 ± 10	64	20***	40
	High surface	86 ± 14**	17	101 ± 19	17	56 ± 20***	15	60 ± 20***	15	14 ± 9	17	6 ± 12***	15	30 ± 13***	18	0.43 ± 0.12***	18	75 ± 15***	21	73***	15
	High WSF	100 ± 11	15	120 ± 12	15	86 ± 9	19	106 ± 9	19	17 ± 7	15	18 ± 5	19	26 ± 7***	20	0.16 ± 0.07	20	92 ± 6	20	0	20
Late exposure 3 dph	Control	98 ± 8	50	123 ± 11	50	86 ± 16	61	103 ± 19	61	20 ± 6	50	16 ± 7	61	12 ± 8	79	0.26 ± 0.07	79	83 ± 8	59	2	61
	Low dose	99 ± 10	37	122 ± 13	37	83 ± 10	49	102 ± 13	49	18 ± 8	47	17 ± 5	47	12 ± 7	59	0.25 ± 0.06	59	83 ± 5	77	0	65
	Medium dose	98 ± 12	40	121 ± 14	40	83 ± 16	50	100 ± 19	50	19 ± 7	40	17 ± 8	50	17 ± 9**	58	0.22 ± 0.08**	58	83 ± 5	60	4	50
	High submerged	98 ± 10	57	122 ± 18	57	75 ± 12***	69	83 ± 15***	69	19 ± 8	57	10 ± 7***	69	23 ± 12***	78	0.24 ± 0.06	78	83 ± 5	78	9*	69
	High surface	98 ± 10	19	119 ± 15	19	70 ± 8***	20	71 ± 10***	20	18 ± 7	19	2 ± 3***	20	28 ± 8***	20	0.22 ± 0.04	20	85 ± 5	19	60***	20
	High WSF	100 ± 10	18	124 ± 9	18	84 ± 10	21	102 ± 11	21	20 ± 6	18	18 ± 5	21	23 ± 8***	20	0.16 ± 0.03***	20	90 ± 5***	19	0	21

* $p < 0.05$.
** $p < 0.001$.
*** $p < 0.0001$.

4.1. Oil droplet fouling

Oil droplet fouling occurred in both *H surf* and *H sub* treatments and consequently increased haddock embryotoxicity by escalating the uptake and prolonging the exposure. Droplet fouling on the submerged exposures show that accumulation of oil droplets was due to the biological characteristics of the haddock embryo and not a surface slick artifact. Unlike other cod fish eggs, haddock have an extra membrane of adhesive material covering the primary egg envelope (Hansen et al., 2018; Morrison et al., 1999; Oppen-Berntsen et al., 1990). The chemical composition of this outer membrane is still unknown. However, it clearly has a hydrophobic interaction with oil, and it is responsible for the accumulation of oil droplets on the eggshell. The outer membrane degrades during the embryo phase, a few days before hatching (Sørhus et al., 2015, 2016a, b). Accordingly, the early egg stages accumulated more oil droplets than the late stages in the present study.

Haddock spawn at depths between 30 and 500 m (Olsen et al., 2010; Solemdal et al., 1997). The eggs have a natural high buoyancy, and all embryonic stages have been observed in the surface in field-based monitoring (Solemdal et al., 1997). Oil droplet fouling can increase the buoyancy of the egg, both by the low density of oil itself, but also by trapping of air bubbles on the chorion (Sørhus et al., 2015). In contrast, we have also observed that haddock eggs with oil droplets become negatively buoyant just before hatching and then sink to the bottom of the exposure tanks (unpublished observations). Similar effects have been observed in oil-exposed mahi-mahi (*Coryphaena hippurus*) (Pasparakis et al., 2017). The mechanism behind this remains unclear, but one possibility is loss of water due to disruption of the perivitelline membrane or disruption of the osmotic control (Pasparakis et al., 2017). Even though we did observe some slick formation as seen in the *H surf* treatment, we argue that this treatment is also the more ecologically relevant exposure. In a situation where crude oil is discharged at depths like in the Deepwater Horizon accident or in a rough sea, oil droplets will be located throughout the water column (Hansen et al., 2019; Nordtug et al., 2011). Consequently, oil droplet fouling increases buoyancy, that might lead to increased speed to the surface and to even greater exposures in the oil slick.

Oil droplet fouling causes transfer of more and higher molecular weight oil components to the embryo (Sørensen et al., 2017). Concentration responses for several end-points indicate that oil compounds entered the embryo. Although the nominal oil concentration in water in *H WSF* were higher than *M* sub treatment, both PAH uptake and *cyp1a* induction were mainly higher in *M* sub treatment compared to *H WSF* treatment especially in the *early* exposure. Interestingly, the composition of PAHs was also different. Few high molecular weight (5–6-rings) PAHs were found in the tissue PAH of the *H WSF* treatment in any exposure. Accordingly, the *H WSF* treatment had very little CYP1A activity (EROD assay) compared to all other treatments where oil droplets were included.

In haddock embryos, oil droplets possibly increase toxicity. First, oil droplet fouling results in prolonged exposure even when transferred to clean water. Second, oil droplets adhered to the chorion may also contribute to transfer of higher molecular-weight, lipophilic compounds like 4–6-ring PAHs that are less available in a water exposure without oil droplets (Sørensen et al., 2017). Enhanced toxicity after direct contact with oil and accumulation on the chorion have also been observed in medaka (*Oryzias latipes*) (Gonzalez-Doncel et al., 2008) and polar cod (Laurel et al., 2019). These results highlight the importance of including mechanically dispersed oil in experimental exposure designs and risk assessment models (Nordtug et al., 2011).

4.2. PAH uptake, Cyp induction and metabolism

We observed delayed expression of *cyp1* paralogs and *abcb1* transporter, higher body burdens of PAHs and lower concentrations of metabolites in early embryos. The difference in the two exposures most likely represents a less developed detoxification system in the early

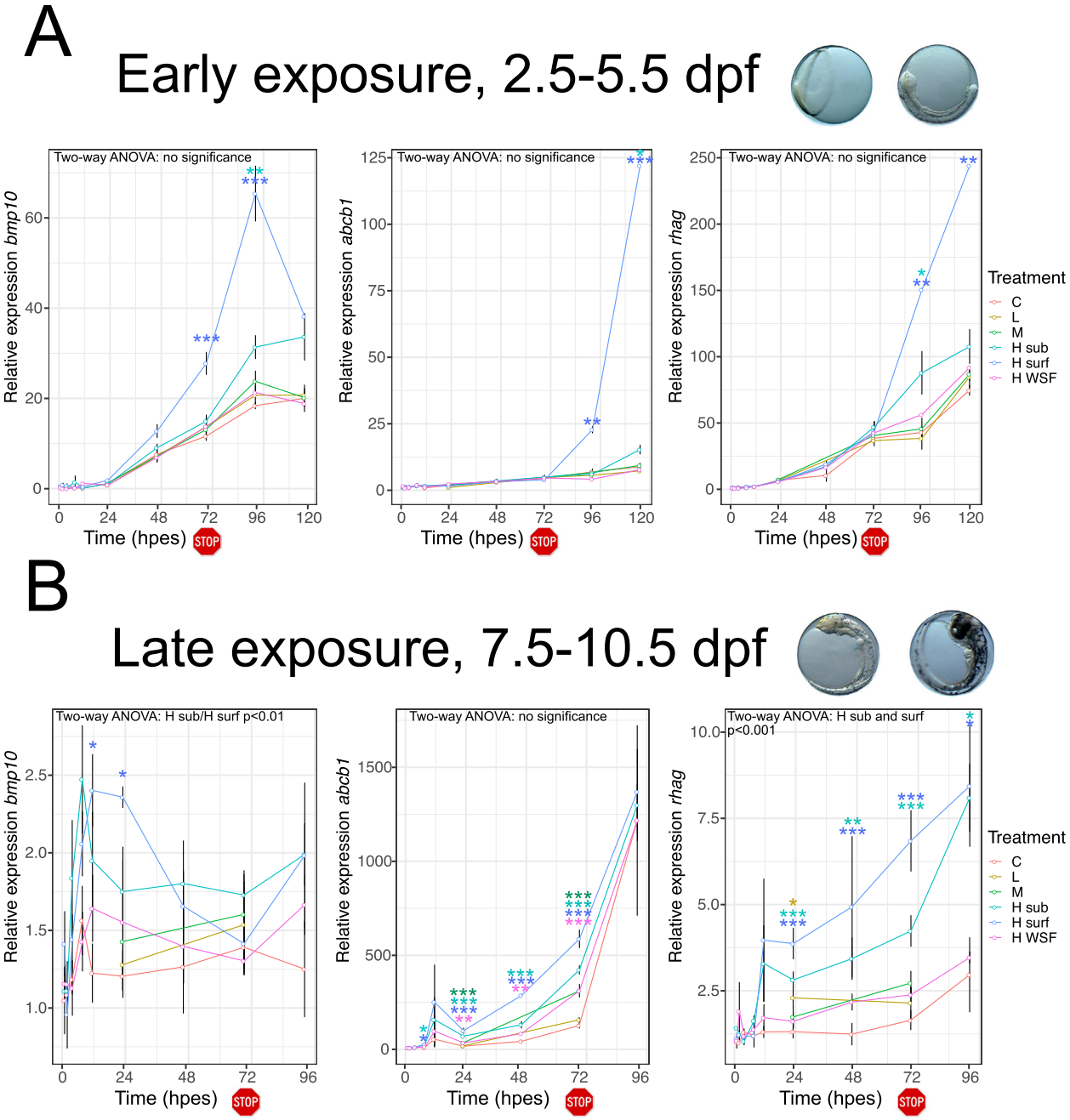

Fig. 7. Relative expression of bmp10, abcb1 and rhag. Relative expression compared to control at exposure start for bmp10, abcb1 and rhag after early (A) and late (B) exposure. Expression was related to control treatment at exposure start to detect both developmental and treatment related expression. Termination of exposure is indicated by a stop icon. Statistical difference to control was tested at each time point with one-way ANOVA with Dunnet's multiple comparisons, and significant differences are indicated by *: $p < 0.05$ or ***: $p < 0.001$. At 120 hpes in the early exposure, only one sample was collected for H surf and H WSF. Error bars represent ±standard deviation. Note: The ranges of the y-axes are not the same for the various panels. dpf: days post fertilization, hpes: hours post exposure start, C: control, L: low treatment, M: medium treatment, H sub: high treatment submerged, H surf: high treatment surface, H WSF: high treatment water soluble fraction.

embryos (Sørhus et al., 2016a). Xenobiotic metabolism is necessary to excrete toxic substances. The liver is the main site for CYP1A activity and detoxification in older fish larvae (Sørhus et al., 2016b). First observation of the rudimentary liver in cod fishes is observed at 30 somite stage (Fridgeirsson, 1978; Hall et al., 2004), approximately 7 dpf in haddock. Expression of *cyp1a* was observed in the skin, cardiac tissues and in the developing liver of Atlantic cod at 8 and 10 dpf (Aranguren-Abadía et al., 2020). Among the thousands of potential PAH and alkyl-PAH metabolites, we used PHE as a model compound to study the metabolic capacity of the haddock embryo. Even though PHE does not induce *cyp1a* itself (Hawkins et al., 2002), it is easily metabolized by CYP1A enzymes present in the tissue (Sørensen et al., 2017). The *late* exposure had more efficient elimination of PAHs evidenced by the immediate strong *cyp1* response resulting in lower peak concentrations of tissue PAHs and higher concentrations of metabolites (e.g. PAH concentrations were approximately 2.5 times lower in *H surf late* compared to *early* exposure). In the *late* exposure *cyp1a*, *cyp1b* and *cyp1c* mRNA were highly and quickly induced, and already after 24 h the metabolic capacity surpassed the uptake rate of PHE in *H surf*. This resulted in a reduced body burden even under continuous exposure. However, we observe accumulation of PHE metabolites suggesting that the rate of excretion does not meet the rate of metabolite formation.

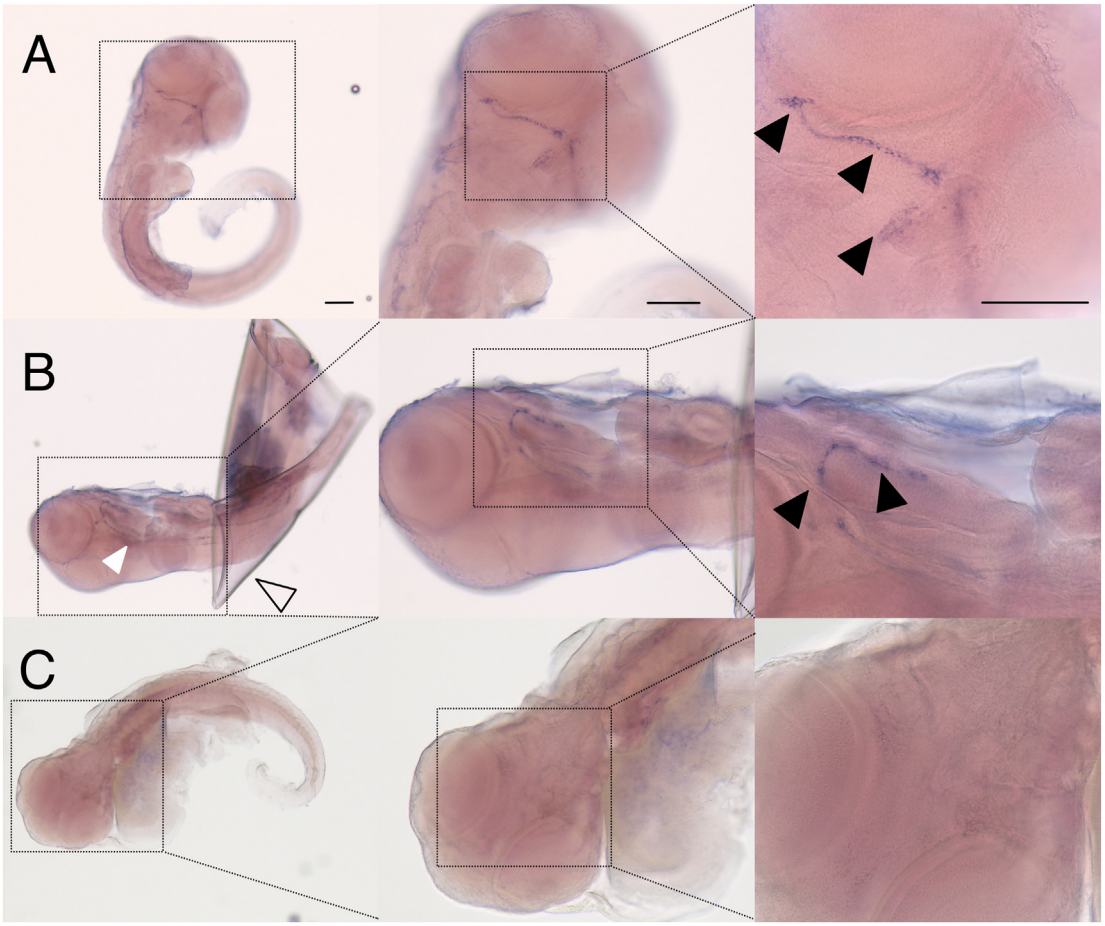

Fig. 8. Whole mount *in situ* hybridization of rhag. Expression pattern of rhag in ventral (A) and lateral (B) view in 10 dpf unexposed embryos of Atlantic haddock. Expression is following the branchial arch. C) No labeling in sense control. Black arrow head: expression of rhag, open arrow: eggshell, white arrow head: unspecific coloration of otoliths.

Our gene expression data suggest that CYP1A is the main detoxification enzyme in *early* embryonic development. The other *cyp1* paralogs investigated, *cyp1b* and *cyp1c*, were not induced until later in the *early* exposure. Increased expression of *cyp1b* unrelated to exposure from 3.5 dpf (24 hpes) emphasizes other developmental roles of CYPs (e.g. steroid biosynthesis and cardiovascular and eye development (Chaudhary et al., 2009; Li et al., 2017)) during early fish development (Goldstone et al., 2010). At 72 hpes a 200 fold up-regulation of *cyp1c* related to development was observed (Fig. S6) and at the same time a strong up-regulation was seen in the treatments. These observations suggest that xenobiotic induction of *cyp1c* is occurring as soon as the organism possesses CYP 1C activity. A delayed oil induced induction of *cyp1b* and *cyp1c* underscore the differences in capability for fish embryos to metabolize xenobiotics depending on their embryonic developmental window. Our results coincide with the findings of (Kuhnert et al., 2017) where the expression of *cyp1b* and *cyp1c* also was delayed compared to *cyp1a* in zebrafish exposed to benzo(*a*)pyrene. We realize that gene expression is a complex process involving gene regulation, differential translation, and peptide stability (Vogel and Marcotte, 2012). Therefore, the gene expression data presented here is merely an indication of enzymatic activity.

While CYP1A appears protective and is necessary for detoxification (Billiard et al., 2006; Mu et al., 2016; Scott et al., 2011; Wincent et al., 2015), it may also result in the production of some reactive toxic metabolites (Wells et al., 1997). Other enzymes can also produce metabolites that can increase the toxicity (Nebert et al., 2004). Several studies have found that hydroxylated PAHs have greater toxic effects than parent compounds (Chibwe et al., 2015; Diamante et al., 2017; Fallahtafti et al., 2012; Schrlau et al., 2017). Bioactivation of PAHs has also been linked to endocrine disruption (Fernandes and Porte, 2013; Hyzd'alova et al., 2018; Pencikova et al., 2019; Sievers et al., 2013; Van de Wiele et al., 2005). Moreover, electrophilic intermediates of PAH metabolism are well known for the formation of hydrophobic DNA adducts and cancer induction (Moorthy et al., 2015). PAH metabolites may also play an important role in cardiotoxicity. PHE and oil are shown to block currents of K^+ through the ERG potassium channel (Brette et al., 2014; Brette et al., 2017). However, the exact mechanism behind how three-ring PAHs are able to block the channel is not well defined (Incardona, 2017). In silico docking models suggest that PHE has the necessary three aromatic rings, but lacks any other functional groups essential for strong blocking capacity to ERG channel (Cavalli et al., 2012; Vandenberg et al., 2012). Other types of membrane ion channels have been intensively studied through the use of PAH metabolites: The 9-hydroxy-PHE metabolite (9-phenanthrol) is a selective and sensitive blocker of the transient receptor potential melastatin 4 channels (TRPM4), a calcium activated cation channel that mediates membrane depolarization (Burris et al., 2015; Guinamard et al., 2014; Hou et al., 2018). Similarly, anthracene-9-carboxylic acid is a commonly used blocker of the calcium-activated chloride channels (CaCCs) (TMEM16A) (Cherian et al., 2015; Ta et al., 2016). The blocking capacity of PAH metabolites to the ERG channels has not yet been studied to our knowledge, but it is possible, if not likely, that critical aspects of crude oil cardiotoxicity are caused by an ERG-blocking PAH metabolite. Taken together we see a need for more studies of the effects of PAH metabolism in oil toxicity. We urge more labs to develop analytical methods able to cover a broad spectra of oil-related metabolites. The latter is a great

methodological challenge due to extreme complexity in the number of metabolites and the lack of available standards.

We show that *cyp1* mRNA induction, content of PAHs in tissue, and PAH metabolites are related to early life stage toxicity in fish, where the amount of mRNA induction and PAH and metabolite concentrations is related to the window of exposure. This observation is in line with an established relationship between toxicity and PAHs in crude oil (Carls and Meador, 2009; Hodson, 2017) and petrogenic substances (Adams et al., 2014; Kamelia et al., 2019; Kamelia et al., 2017). However, there are multiple toxic components in crude oil apart from PAHs that can induce toxicity in early life stages of fish (Meador and Nahrgang, 2019; Sørensen et al., 2019). Therefore, there is a need for more fractionation studies and effect directed analysis (EDA) to increase our understanding of the additive and synergetic interactions of complex mixtures of petroleum hydrocarbons.

4.3. Morphological abnormalities

The large differences in morphological abnormalities after *early* vs *late* exposure show the importance of timing of exposure. The *early* exposure has major consequences for formation of organs by interfering with the developmental signaling pathways, while *late* exposure mainly shows effect on organism condition possibly downstream of cardiofunctional defects.

The eye abnormalities were most likely downstream of both circulation defects and altered CYP-regulation. Crude oil-induced eye developmental defects are well documented. Both reduced eye size (anapthalmia) and reduced size with abnormalities (microphtalmia) are observed (Incardona et al., 2014; Lie et al., 2019; Magnuson et al., 2018). In the present study, eye size was mainly affected in the *early* exposure, where we found the most severe developmental and functional abnormalities. Zebrafish with no cardiac function (*tnnt* morpholinos) mimic the oil-induced reduction in eye size (Incardona et al., 2004), suggesting that anapthalmia is secondary to circulatory defects. However, it is also suggested that abnormal cyp-balance disrupts retinoic acid signaling pathway through disturbance of Cyp26, leading to abnormal eye development (Lie et al., 2019; Yamamoto et al., 2000). Another Cyp enzyme, CYP1B, is also involved in eye development (regulating ocular fissure closure) through both retinoic acid-dependent and -independent pathways (Chambers et al., 2007; Williams et al., 2017). Affirmative of a non-toxicological function of CYP1B was the general increase in expression of *cyp1b* beginning at 3.5 dpf (24 hpes). Overexpression of *cyp1b* causes irregular eye shape referred to as coloboma (Chambers et al., 2007; Williams et al., 2017). The *late* exposure animals possessed less severe abnormalities in general. However, the *H sub* and *H surf* treatments still showed excessive incidence of eye abnormalities (irregular eye shape) which could be connected to the increased *cyp1b* expression. These findings are in line with findings that proper closure of the ocular fissure is disrupted by overexpression of *cyp1b* (Chambers et al., 2007; Williams et al., 2017). Thus, inappropriate oil induced expression of *cyp1b* in the eyes could be an additional mechanism leading to abnormal eye development.

The craniofacial abnormalities observed in our exposed animals are potentially due to both disruption of jaw and pharyngeal arch formation and reduced outgrowth linked to abnormal craniofacial muscle function. Expression of *cyp1b* was found in pharyngeal arches of zebrafish exposed to PCB 126 and TCDD (Timme-Laragy et al., 2008; Yin et al., 2008), and the injection of human *cyp1b* mRNA resulted in disruption of neural crest-derived jaw and pharyngeal arch formation (Williams et al., 2017). Furthermore, muscle contraction is mandatory for proper stacking of chondrocytes and outgrowth of craniofacial cartilages (Shwartz et al., 2012). Crude oil disrupts cardiac muscle function (Brette et al., 2014; Brette et al., 2017; Incardona et al., 2014), and jaw spasms observed in previous studies suggest a similar effect on the craniofacial muscles. Impairment of craniofacial muscles might explain the high prevalence of craniofacial abnormalities in the *late* exposure. In conclusion, the tight correlation between *cyp1b* expression and oil induced eye and jaw deformities suggests that inappropriate expression of *cyp1b* in oil-exposed animals are directly linked to abnormal eye and jaw development.

4.4. Cardiac morphological defects

The severely malformed and small hearts after *early* exposure imply multiple impacts on cardiac formation and early development. The reduced heart size in the *late* exposure suggests an impact on late development and especially cardiomyocyte proliferation.

Oil induced up-regulation of *bmp10* was observed even before initiation of first heart beat. A circulation- and time-independent expression of *bmp10* suggests a direct effect of crude oil on calcium homeostasis. Several signaling pathways linked to cardiac development and proliferation are impacted by the complexity of crude oil exposure, including calcium-regulated pathways (Sørhus et al., 2017; Xu et al., 2017), AhR (Yin et al., 2008) and retinoic acid-dependent (Lie et al., 2019) pathways. Disruption of intracellular calcium levels has been shown to reduce cardiomyocyte proliferation leading to smaller ventricles (Ebert et al., 2005; Rottbauer et al., 2001), suggesting that ventricular proliferation is calcium controlled. BMP10 is a calcium-regulated signaling molecule involved in cardiogenesis (Huang et al., 2012; Wamhoff et al., 2004; Wamhoff et al., 2006) and is thought to orchestrate several major key cardiogenic factors and play a part in ventricular cell proliferation (Chen et al., 2004; Shou et al., 1998). In the current study, we observed an up-regulation of *bmp10* regardless of timing of exposure. However, the developmental consequences of timing of an inappropriate gene regulation is essential. In the *early* exposure, the initiation of *bmp10* up-regulation was occurring at cardiac cone stage (72 hpes). At this stage of development asymmetric Bmp signaling (in particular BMP4) in the cardiac primordium is involved in the looping of the heart (Chocron et al., 2007; Huang et al., 2012; Lombardo et al., 2019). An overexpression of *bmp10* in the cardiac primordium may therefore disrupt left/right looping of the heart. At the start of the *late* exposure, the looping process was already initiated, and the heart was functionally beating. Consequently, we observed less severe effect on looping, while growth of the heart was altered. Reduced size of the ventricle was observed in both *H sub* and *H surf*, as well as an overall up-regulation of *bmp10*. The up-regulation of *bmp10* may be consequential for the reduced ventricle size in exposed larvae from the late embryonic stages. Taken together, the observations from *early* and *late* exposures support the idea that oil components have a circulation-independent direct effect on calcium homeostasis likely disrupting cardiac development and proliferation indicated by the up-regulation of *bmp10*.

4.5. Cardiac functional defects

The cardiac functional defects post-exposure were linked to irreversible morphological changes and reversible effects of circulating crude oil components. Reduced contractility and non-contracting ventricles (SiV phenotype) were traits found in both *early* and *late* exposures. Functional defects in the *early* exposure could originate from irreversible morphological changes (severely malformed ventricles) but could also stem from consumption of oil components stored in the yolk sac after hatching as observed in previous studies (Sørhus et al., 2016b; Vanleeuwen et al., 1985). The *late* exposure animals, on the other hand, had normally shaped but often smaller ventricles. The contractility abnormalities in the *late* exposure most likely stem from consumption of components stored in the yolk sac.

A suite of defects downstream of cardiac dysfunction has been described for oil-exposed developing fish, including edema (Incardona, 2017; Incardona and Scholz, 2016). Edema formation measured included both pericardial and yolk sac edemas, and may be due to i) irreversible morphological cardiac deformities that alter the cardiac function later in life and ii) oil components that can directly alter the

electrophysiological activity (contractility and rhythm) of the developing heart (Brette et al., 2014; Brette et al., 2017; Incardona, 2017). Circulatory defects may also affect distribution of lipids from the yolk which in turn may affect growth in later stages. Polar cod exposed to transient low concentrations of oil induced dysregulation of lipid metabolism and reduced growth in morphologically normal juveniles (Laurel et al., 2019). We observed a reduced yolk utilization in *H surf* in the *early* exposure, suggesting that these embryos were deprived of essential yolk-based lipids. Furthermore, the reduced yolk utilization seems to be associated with heart rate, and thus, dependent on circulation. Accordingly, the treatment group with tachycardia had highly increased yolk utilization (*H WSF*), while the treatment group with bradycardia (*H surf*) had severely reduced yolk utilization. Overall, cardiocirculatory defects during embryonic development could be sufficient to impact growth and could be consequential for individual fitness at juvenile and adult stages.

4.6. Osmoregulation

Up-regulation of *rhag* suggests that osmoregulatory cells are impacted by oil exposure. Osmoregulation can be disrupted by circulatory defects (Miyanishi et al., 2013), or directly affected by oil components (Sørhus et al., 2017). In adult fish, the main localization for osmoregulation, gas exchange and transport of ammonium are in the gills (Evans et al., 2005) in osmoregulatory cells called mitochondrial rich cells (MRCs) (Evans et al., 2005; Hiroi et al., 2005; Hirose et al., 2003; Shelbourne, 1957). In 10 dpf haddock, expression of *rhag* was found in the branchial arches (primordial gills), in close proximity to expected localization of MRCs (Zimmer et al., 2014; Zimmer et al., 2017). Therefore, oil induced up-regulation of *rhag* in MRCs could impact osmoregulation in oil exposed fish. This finding coincides with expression of *rhag* in mahi-mahi at approximately the same developmental time point (Wang et al., 2019). In both *early* and *late* exposures, *rhag* seemed to track more with the peak of *cyp1a* induction and *abcb1* transporter. This could indicate that energy for CYP1A-mediated PAH metabolism is derived from amino acids (Pasparakis et al., 2016), generating nitrogenous waste as also suggested by Wang et al. (2019). Thus, an increased amount of ammonium waste could also affect osmoregulation capacity of MRCs and consequently lead to increased edema formation.

5. Conclusion

In this study we showed that oil droplet fouling occurred throughout the whole water column and contributed to increased PAH uptake and embryotoxicity. Oil droplet fouling makes the haddock embryo extremely vulnerable to even short, low concentration oil exposures. The high bioaccumulation of PAHs and lower concentrations of metabolites in the *early* exposure reflects a less developed response system that possibly has an exacerbating toxic effect in early embryos. Short term exposures prior to and after onset of heart beat and frequent sampling regime enabled us to establish direct and downstream effects of crude oil exposure. The relatively rapid and circulatory-independent response in *bmp10* regulation suggested direct effects on calcium homeostasis affecting calcium-regulated developmental pathways, including cardiogenesis. Similarly, we propose that abnormal regulation of *cyp1b* due to oil exposure may affect eye and jaw development. Expression of *rhag* indicates a direct oil effect on osmoregulatory cells and osmoregulation. We recognize that oil is a complex mixture of many potential toxic components. Yet, the strong correlations among PAH uptake, *cyp1a* induction, metabolite formation and malformations suggest that body burden of PAHs in tissue remains a good metric for oil toxicity.

Our findings are adding more knowledge about development stage-dependent effects of crude oil exposure. Thus, we provide more knowledge and detail to several existing adverse outcome pathways of crude oil toxicity.

Supplementary data to this article can be found online at https://doi.org/10.1016/j.scitotenv.2020.143896.

CRediT authorship contribution statement

Elin Sørhus: Conceptualization, Methodology, Investigation, Formal analysis, Data curation, Writing – original draft. **Carey E. Donald:** Formal analysis, Data curation, Writing – original draft. **Denis da Silva:** Formal analysis, Data curation, Resources. **Anders Thorsen:** Conceptualization, Methodology, Resources. **Ørjan Karlsen:** Conceptualization, Methodology, Investigation. **Sonnich Meier:** Conceptualization, Methodology, Investigation, Formal analysis, Data curation, Writing – original draft.

Declaration of competing interest

The authors declare no competing financial interests.

Acknowledgements

We would like to acknowledge Stig Ove Utskot and Tobias Hukset for breeding and management of the fish, Charlotte Nakken for technical assistance with the metabolite data, Prescilla Perrichon for discussion of the data and review of the manuscript and Karen Peck for a thorough review of the manuscript. This work was financed by the Research Council of Norway (EGGTOX: Unraveling the mechanistic effects of crude oil toxicity during early life stages of cold-water marine teleosts (Project # 267820), www.forskningsradet.no) and the Institute of Marine Research, Norway. The funders had no role in study design, data collection and analysis, decision to publish, or preparation of the manuscript.

References

Abramyan, J., 2019. Hedgehog signaling and embryonic craniofacial disorders. J. Dev. Biol. 7.

Adams, J., Bornstein, J.M., Munno, K., Hollebone, B., King, T., Brown, R.S., Hodson, P.V., 2014. Identification of compounds in heavy fuel oil that are chronically toxic to rainbow trout embryos by effects-driven chemical fractionation. Environ. Toxicol. Chem. 33, 825–835.

Andres-Delgado, L., Mercader, N., 2016. Interplay between cardiac function and heart development. BBA-Mol. Cell. Res. 1863, 1707–1716.

Aranguren-Abadía, L., Donald, C.E., Eilertsen, M., Gharbi, N., Tronci, V., Sørhus, E., Mayer, P., Nilsen, T.O., Meier, S., Goksøyr, A., Karlsen, O.A., 2020. Expression and localization of the aryl hydrocarbon receptors and cytochrome P450 1A during early development of Atlantic cod (Gadus morhua). Aquat. Toxicol. 226, 105558.

Beyer, J., Jonsson, G., Porte, C., Krahn, M.M., Ariese, F., 2010. Analytical methods for determining metabolites of polycyclic aromatic hydrocarbon (PAH) pollutants in fish bile: a review. Environ. Toxicol. Pharmacol. 30, 224–244.

Billiard, S.M., Timme-Laragy, A.R., Wassenberg, D.M., Cockman, C., Di Giulio, R.T., 2006. The role of the aryl hydrocarbon receptor pathway in mediating synergistic developmental toxicity of polycyclic aromatic hydrocarbons to zebrafish. Toxicol. Sci. 92, 526–536.

Brette, F., Machado, B., Cros, C., Incardona, J.P., Scholz, N.L., Block, B.A., 2014. Crude oil impairs cardiac excitation-contraction coupling in fish. Science 343, 772–776.

Brette, F., Shiels, H.A., Galli, G.L., Cros, C., Incardona, J.P., Scholz, N.L., Block, B.A., 2017. A novel cardiotoxic mechanism for a pervasive global pollutant. Sci. Rep. 7, 41476.

Burris, S.K., Wang, Q., Bulley, S., Neeb, Z.P., Jaggar, J.H., 2015. 9-Phenanthrol inhibits recombinant and arterial myocyte TMEM16A channels. Br. J. Pharmacol. 172, 2459–2468.

Caner, T., Abdulnour-Nakhoul, S., Brown, K., Islam, M.T., Hamm, L.L., Nakhoul, N.L., 2015. Mechanisms of ammonia and ammonium transport by rhesus-associated glycoproteins. Am. J. Physiol.-Cell Physiol. 309, C747–C758.

Carls, M.G., Meador, J.P., 2009. A perspective on the toxicity of petrogenic PAHs to developing fish embryos related to environmental chemistry. Hum. Ecol. Risk. Assess. 15, 1084–1098.

Carroll, J., Vikebo, F., Howell, D., Broch, O.J., Nepstad, R., Augustine, S., Skeie, G.M., Bast, R., Juselius, J., 2018. Assessing impacts of simulated oil spills on the Northeast Arctic cod fishery. Mar. Pollut. Bull. 126, 63–73.

Cavalli, A., Buonfiglio, R., Ianni, C., Masetti, M., Ceccarini, L., Caves, R., Chang, M.W., Mitcheson, J.S., Roberti, M., Recanatini, M., 2012. Computational design and discovery of "minimally structured" hERG blockers. J. Med. Chem. 55, 4010–4014.

Chambers, D., Wilson, L., Maden, M., Lumsden, A., 2007. RALDH-independent generation of retinoic acid during vertebrate embryogenesis by CYP1B1. Development 134, 1369–1383.

Chaudhary, K.R., Batchu, N., Seubert, J.M., 2009. Cytochrome P450 enzymes and the heart. IUBMB Life 61, 954–960.

Chen, H.Y., Shi, S., Acosta, L., Li, W.M., Lu, J., Bao, S.D., Chen, Z.A., Yang, Z.C., Schneider, M.D., Chien, K.R., Conway, S.J., Yoder, M.C., Haneline, L.S., Franco, D., Shou, W.N., 2004. BMP10 is essential for maintaining cardiac growth during murine cardiogenesis. Development 131, 2219–2231.

Cherian, O.L., Menini, A., Boccaccio, A., 2015. Multiple effects of anthracene-9-carboxylic acid on the TMEM16B/anoctamin2 calcium-activated chloride channel. Biochim. Biophys. Acta 1848, 1005–1013.

Chibwe, L., Geier, M.C., Nakamura, J., Tanguay, R.L., Aitken, M.D., Simonich, S.L., 2015. Aerobic bioremediation of PAH contaminated soil results in increased genotoxicity and developmental toxicity. Environ. Sci. Technol. 49, 13889–13898.

Chocron, S., Verhoeven, M.C., Rentzsch, F., Hammerschmidt, M., Bakkers, J., 2007. Zebrafish Bmp4 regulates left-right asymmetry at two distinct developmental time points. Dev. Biol. 305, 577–588.

Choudhuri, S., Klaassen, C.D., 2006. Structure, function, expression, genomic organization, and single nucleotide polymorphisms of human ABCB1 (MDR1), ABCC (MRP), and ABCG2 (BCRP) efflux transporters. Int. J. Toxicol. 25, 231–259.

Cresci, A., Browman, H.I., Skiftesvik, A.B., Shema, S., Bjelland, R., Durif, C., Foretich, M., Di Persia, C., Lucchese, V., Vikebø, F., Sorhus, E., 2020. Effects of exposure to low concentrations of oil on expression of cytochrome P4501a and routine swimming speed of Atlantic haddock (Melanogrammus aeglefinus) larvae in situ. Environ. Sci. Technol 54, 13879–13887.

Delling, M., DeCaen, P.G., Doerner, J.F., Febvay, S., Clapham, D.E., 2013. Primary cilia are specialized calcium signalling organelles. Nature 504, 311–314.

Diamante, G., do Amaral, E.S.M.G., Menjivar-Cervantes, N., Xu, E.G., Volz, D.C., Dias Bainy, A.C., Schlenk, D., 2017. Developmental toxicity of hydroxylated chrysene metabolites in zebrafish embryos. Aquat. Toxicol. 189, 77–86.

Ebert, A.M., Hume, G.L., Warren, K.S., Cook, N.P., Burns, C.G., Mohideen, M.A., Siegal, G., Yelon, D., Fishman, M.C., Garrity, D.M., 2005. Calcium extrusion is critical for cardiac morphogenesis and rhythm in embryonic zebrafish hearts. Proc. Natl. Acad. Sci. USA 102, 17705–17710.

Evans, D.H., Piermarini, P.M., Choe, K.P., 2005. The multifunctional fish gill: dominant site of gas exchange, osmoregulation, acid-base regulation, and excretion of nitrogenous waste. Physiol. Rev. 85, 97–177.

Fallahtafti, S., Rantanen, T., Brown, R.S., Snieckus, V., Hodson, P.V., 2012. Toxicity of hydroxylated alkyl-phenanthrenes to the early life stages of Japanese medaka (*Oryzias latipes*). Aquat. Toxicol. 106–107, 56–64.

Fernandes, D., Porte, C., 2013. Hydroxylated PAHs alter the synthesis of androgens and estrogens in subcellular fractions of carp gonads. Sci. Total Environ. 447, 152–159.

Fridgeirsson, E., 1978. Embryonic development of five species of gadoid fishes in Icelandic waters. Rit Fiskeideildar 5, 1–68.

Goksøyr, A., 1995. Use of cytochrome P450 1A (CYP1A) in fish as a biomarker of aquatic pollution. Arch. Toxicol. Suppl. 17, 80–95.

Goksoyr, A., Andersson, T., Hansson, T., Klungsoyr, J., Zhang, Y., Forlin, L., 1987. Species characteristics of the hepatic xenobiotic and steroid biotransformation systems of two teleost fish, Atlantic cod (Gadus morhua) and rainbow trout (Salmo gairdneri). Toxicol. Appl. Pharmacol. 89, 347–360.

Goldstone, J.V., McArthur, A.G., Kubota, A., Zanette, J., Parente, T., Jonsson, M.E., Nelson, D.R., Stegeman, J.J., 2010. Identification and developmental expression of the full complement of Cytochrome P450 genes in Zebrafish. BMC Genomics 11, 643.

Gonzalez-Doncel, M., Gonzalez, L., Fernandez-Torija, C., Navas, J.M., Tarazona, J.V., 2008. Toxic effects of an oil spill on fish early life stages may not be exclusively associated to PAHs: studies with prestige oil and medaka (*Oryzias latipes*). Aquat. Toxicol. 87, 280–288.

Gonzalez-Doncel, M., San Segundo, L., Sastre, S., Tarazona, J.V., Torija, C.F., 2011. Dynamics of BNF-induced in vivo ethoxyresorufin-O-deethylase (EROD) activity during embryonic development of medaka (Oryzias latipes). Aquat. Toxicol. 105, 421–427.

Guinamard, R., Hof, T., Del Negro, C.A., 2014. The TRPM4 channel inhibitor 9-phenanthrol. Br. J. Pharmacol. 171, 1600–1613.

Hall, T.E., Cole, N.J., Johnston, I.A., 2003. Temperature and the expression of seven muscle-specific protein genes during embryogenesis in the Atlantic cod Gadus morhua L. J. Exp. Biol. 206, 3187–3200.

Hall, T.E., Smith, P., Johnston, I.A., 2004. Stages of embryonic development in the Atlantic cod Gadus morhua. J. Morphol. 259, 255–270.

Hansen, B.H., Sørensen, L., Carvalho, P.A., Meier, S., Booth, A.M., Altin, D., Farkas, J., Nordtug, T., 2018. Adhesion of mechanically and chemically dispersed crude oil droplets to eggs of Atlantic cod (Gadus morhua) and haddock (Melanogrammus aeglefinus). Sci. Total Environ. 640-641, 138–143.

Hansen, B.H., Salaberria, I., Read, K.E., Wold, P.A., Hammer, K.M., Olsen, A.J., Altin, D., Overjordet, I.B., Nordtug, T., Bardal, T., Kjorsvik, E., 2019. Developmental effects in fish embryos exposed to oil dispersions — the impact of crude oil micro-droplets. Mar. Environ. Res. 150.

Hawkins, S.A., Billiard, S.M., Tabash, S.P., Brown, R.S., Hodson, P.V., 2002. Altering cytochrome P4501A activity affects polycyclic aromatic hydrocarbon metabolism and toxicity in rainbow trout (Oncorhynchus mykiss). Environ. Toxicol. Chem. 21, 1845–1853.

Heintz, R.A., Rice, S.D., Wertheimer, A.C., Bradshaw, R.F., Thrower, F.P., Joyce, J.E., Short, J.W., 2000. Delayed effects on growth and marine survival of pink salmon Oncorhynchus gorbuscha after exposure to crude oil during embryonic development. Mar. Ecol. Prog. Ser. 208, 205–216.

Hicken, C.E., Linbo, T.L., Baldwin, D.H., Willis, M.L., Myers, M.S., Holland, L., Larsen, M., Stekoll, M.S., Rice, S.D., Collier, T.K., Scholz, N.L., Incardona, J.P., 2011. Sublethal exposure to crude oil during embryonic development alters cardiac morphology and reduces aerobic capacity in adult fish. Proc. Natl. Acad. Sci. USA 108, 7086–7090.

Hiroi, J., Miyazaki, H., Katoh, F., Ohtani-Kaneko, R., Kaneko, T., 2005. Chloride turnover and ion-transporting activities of yolk-sac preparations (yolk balls) separated from Mozambique tilapia embryos and incubated in freshwater and seawater. J. Exp. Biol. 208, 3851–3858.

Hirose, S., Kaneko, T., Naito, N., Takei, Y., 2003. Molecular biology of major components of chloride cells. Comp. Biochem. Phys. B 136, 593–620.

Hodson, P.V., 2017. The toxicity to fish embryos of PAH in crude and refined oils. Arch. Environ. Contam. Toxicol. 73, 12–18.

Hou, J.W., Fei, Y.D., Li, W., Chen, Y.H., Wang, Q., Xiao, Y., Wang, Y.P., Li, Y.G., 2018. The transient receptor potential melastatin 4 channel inhibitor 9-phenanthrol modulates cardiac sodium channel. Br. J. Pharmacol. 175, 4325–4337.

Huang, J.H., Elicker, J., Bowens, N., Liu, X., Cheng, L., Cappola, T.P., Zhu, X.H., Parmacek, M.S., 2012. Myocardin regulates BMP10 expression and is required for heart development. J. Clin. Invest. 122, 3678–3691.

Hyzd'alova, M., Pivnicka, J., Zapletal, O., Vazquez-Gomez, G., Matthews, J., Neca, J., Pencikova, K., Machala, M., Vondracek, J., 2018. Aryl hydrocarbon receptor-dependent metabolism plays a significant role in estrogen-like effects of polycyclic aromatic hydrocarbons on cell proliferation. Toxicol. Sci. 165, 447–461.

Incardona, J.P., 2017. Molecular mechanisms of crude oil developmental toxicity in fish. Arch. Environ. Contam. Toxicol. 73, 19–32.

Incardona, J.P., Scholz, N.L., 2016. The influence of heart developmental anatomy on cardiotoxicity-based adverse outcome pathways in fish. Aquat. Toxicol. 177, 515–525.

Incardona, J.P., Collier, T.K., Scholz, N.L., 2004. Defects in cardiac function precede morphological abnormalities in fish embryos exposed to polycyclic aromatic hydrocarbons. Toxicol. Appl. Pharmacol. 196, 191–205.

Incardona, J.P., Carls, M.G., Day, H.L., Sloan, C.A., Bolton, J.L., Collier, T.K., Scholz, N.L., 2009. Cardiac arrhythmia is the primary response of embryonic Pacific herring (*Clupea pallasi*) exposed to crude oil during weathering. Environ. Sci. Technol. 43, 201–207.

Incardona, J.P., Gardner, L.P., Linbo, T.L., Brown, T.L., Esbaugh, A.J., Mager, E.M., Stieglitz, J.D., French, B.L., Labenia, J.S., Laetz, C.A., Tagal, M., Sloan, C.A., Elizur, A., Benetti, D.D., Grosell, M., Block, B.A., Scholz, N.L., 2014. *Deepwater Horizon* crude oil impacts the developing hearts of large predatory pelagic fish. Proc. Natl. Acad. Sci. USA 111, E1510–E1518.

Johann, S., Nüßer, L., Goßen, M., Hollert, H., Seiler, T.B., 2020. Differences in biomarker and behavioral responses to native and chemically dispersed crude and refined fossil oils in zebrafish early life stages. Sci. Total Environ. 709, 136174.

Kamelia, L., Louisse, J., de Haan, L., Rietjens, I., Boogaard, P.J., 2017. Prenatal developmental toxicity testing of petroleum substances: application of the mouse embryonic stem cell test (EST) to compare in vitro potencies with potencies observed in vivo. Toxicol. in Vitro 44, 303–312.

Kamelia, L., de Haan, L., Ketelslegers, H.B., Rietjens, I., Boogaard, P.J., 2019. In vitro prenatal developmental toxicity induced by some petroleum substances is mediated by their 3- to 7-ring PAH constituent with a potential role for the aryl hydrocarbon receptor (AhR). Toxicol. Lett. 315, 64–76.

Kimmel, C.B., Miller, C.T., Moens, C.B., 2001. Specification and morphogenesis of the zebrafish larval head skeleton. Dev. Biol. 233, 239–257.

Kimura, Y., Morita, S.Y., Matsuo, M., Ueda, K., 2007. Mechanism of multidrug recognition by MDR1/ABCB1. Cancer Sci. 98, 1303–1310.

Kuhnert, A., Vogs, C., Seiwert, B., Aulhorn, S., Altenburger, R., Hollert, H., Kuster, E., Busch, W., 2017. Biotransformation in the zebrafish embryo -temporal gene transcription changes of cytochrome P450 enzymes and internal exposure dynamics of the AhR binding xenobiotic benz[a]anthracene. Environ. Pollut. 230, 1–11.

Laurel, B.J., Iseri, P., Spencer, M.L., Hutchinson, G., Nordtug, T., Donald, C.E., Meier, S., Allan, S.E., Boyd, D.T., Ylitalo, G.M., Cameron, J.R., French, B.L., Linbo, T.L., Scholz, N.L., Incardona, J.P., 2019. Embryonic crude oil exposure impairs growth and lipid allocation in a keystone arctic forage fish. iScience 19, 1101–1113.

Li, F., Zhu, W.F., Gonzalez, F.J., 2017. Potential role of CYP1B1 in the development and treatment of metabolic diseases. Pharmacol. Ther. 178, 18–30.

Lie, K.K., Meier, S., Sørhus, E., Edvardsen, R.B., Karlsen, O., Olsvik, P.A., 2019. Offshore crude oil disrupts retinoid signaling and eye development in larval Atlantic haddock. Front. Mar. Sci. 6.

Lombardo, V.A., Heise, M., Moghtadaei, M., Bornhorst, D., Manner, J., Abdelilah-Seyfried, S., 2019. Morphogenetic control of zebrafish cardiac looping by bmp signaling. Development 146.

Magnuson, J.T., Khursigara, A.J., Allmon, E.B., Esbaugh, A.J., Roberts, A.P., 2018. Effects of Deepwater Horizon crude oil on ocular development in two estuarine fish species, red drum (Sciaenops ocellatus) and sheepshead minnow (Cyprinodon variegatus). Ecotoxicol. Environ. Saf. 166, 186–191.

Marris, C.R., N., K.S., Miller, M.R., Incardona, J.P., Brette, F., C., H.J., Sørhus, E., Shiels, H.A., 2019. Polyaromatic hydrocarbons in pollution: a heart-breaking matter. J. Physiol. 598, 227–247.

McGruer, V., Pasparakis, C., Grosell, M., Stieglitz, J.D., Benetti, D.D., Greer, J.B., Schlenk, D., 2019. Deepwater Horizon crude oil exposure alters cholesterol biosynthesis with implications for developmental cardiotoxicity in larval mahi-mahi (Coryphaena hippurus). Comp. Biochem. Phys. C 220, 31–35.

Meador, J.P., Nahrgang, J., 2019. Characterizing crude oil toxicity to early-life stage fish based on a complex mixture: are we making unsupported assumptions? Environ. Sci. Technol. 53, 11080–11092.

Miyanishi, H., Okubo, K., Kaneko, T., Takei, Y., 2013. Role of cardiac natriuretic peptides in seawater adaptation of medaka embryos as revealed by loss-of-function analysis. Am. J. Physiol. Renal Physiol. 304, R423–R434.

Moorthy, B., Chu, C., Carlin, D.J., 2015. Polycyclic aromatic hydrocarbons: from metabolism to lung cancer. Toxicol. Sci. 145, 5–15.

Morrison, C., Bird, C., O'Neil, D., Leggiadro, C., Martin-Robichaud, D., Rommens, M., Waiwood, K., 1999. Structure of the egg envelope of the haddock, *Melanogrammus aeglefinus*, and effects of microbial colonization during incubation. Can. J. Zool. 77, 890–901.

Mu, J., Jin, F., Wang, J., Wang, Y., Cong, Y., 2016. The effects of CYP1A inhibition on alkylphenanthrene metabolism and embryotoxicity in marine medaka (Oryzias melastigma). Environ. Sci. Pollut. Res. Int. 23, 11289–11297.

Nebert, D.W., Dalton, T.P., Okey, A.B., Gonzalez, F.J., 2004. Role of aryl hydrocarbon receptor-mediated induction of the CYP1 enzymes in environmental toxicity and cancer. J. Biol. Chem. 279, 23847–23850.

Nordtug, T., Olsen, A.J., Altin, D., Meier, S., Overrein, I., Hansen, B.H., Johansen, O., 2011. Method for generating parameterized ecotoxicity data of dispersed oil for use in environmental modelling. Mar. Pollut. Bull. 62, 2106–2113.

Olsen, E., Aanes, S., Mehl, S., Holst, J.C., Aglen, A., Gjosaeter, H., 2010. Cod, haddock, saithe, herring, and capelin in the Barents Sea and adjacent waters: a review of the biological value of the area. ICES J. Mar. Sci. 67, 87–101.

Oppen-Berntsen, D.O., Helvik, J.V., Walther, B.T., 1990. The major structural proteins of cod (Gadus morhua) eggshells and protein crosslinking during teleost egg hardening. Dev. Biol. 137, 258–265.

Pampanin, D.M., Kemppainen, E.K., Skogland, K., Jorgensen, K.B., Sydnes, M.O., 2016. Investigation of fixed wavelength fluorescence results for biliary metabolites of polycyclic aromatic hydrocarbons formed in Atlantic cod (Gadus morhua). Chemosphere 144, 1372–1376.

Pangrekar, J., Kole, P.L., Honey, S.A., Kumar, S., Sikka, H.C., 2003. Metabolism of phenanthrene by brown bullhead liver microsomes. Aquat. Toxicol. 64, 407–418.

Pasparakis, C., Mager, E.M., Stieglitz, J.D., Benetti, D., Grosell, M., 2016. Effects of Deepwater horizon crude oil exposure, temperature and developmental stage on oxygen consumption of embryonic and larval mahi-mahi (Coryphaena hippurus). Aquat. Toxicol. 181, 113–123.

Pasparakis, C., Sweet, L.E., Stieglitz, J.D., Benetti, D., Casente, C.T., Roberts, A.P., Grosell, M., 2017. Combined effects of oil exposure, temperature and ultraviolet radiation on buoyancy and oxygen consumption of embryonic mahi-mahi, *Coryphaena hippurus*. Aquat. Toxicol. 191, 113–121.

Pasparakis, C., Esbaugh, A.J., Burggren, W., Grosell, M., 2019. Impacts of Deepwater horizon oil on fish. Comp. Biochem. Phys. C 224, 108558.

Pencikova, K., Ciganek, M., Neca, J., Illes, P., Dvorak, Z., Vondracek, J., Machala, M., 2019. Modulation of endocrine nuclear receptor activities by polyaromatic compounds present in fractionated extracts of diesel exhaust particles. Sci. Total Environ. 677, 626–636.

Petersen, G.I., Kristensen, P., 1998. Bioaccumulation of lipophilic substances in fish early life stages. Environ. Toxicol. Chem. 17, 1385–1395.

Rottbauer, W., Baker, K., Wo, Z.G., Mohideen, M.A.P.K., Cantiello, H.F., Fishman, M.C., 2001. Growth and function of the embryonic heart depend upon the cardiac-specific L-type calcium channel alpha 1 subunit. Dev. Cell 1, 265–275.

Schrlau, J.E., Kramer, A.L., Chlebowski, A., Truong, L., Tanguay, R.L., Simonich, S.L.M., Semprini, L., 2017. Formation of developmentally toxic phenanthrene metabolite mixtures by Mycobacterium sp. ELW1. Environ. Sci. Technol. 51, 8569–8578.

Scott, J.A., Incardona, J.P., Pelkki, K., Shepardson, S., Hodson, P.V., 2011. AhR2-mediated, CYP1A-independent cardiovascular toxicity in zebrafish (Danio rerio) embryos exposed to retene. Aquat. Toxicol. (Amsterdam, Netherlands) 101, 165–174.

Sette, C.B., Pedrete Tde, A., Felizzola, J., Nudi, A.H., Scofield Ade, L., Wagener Ade, L., 2013. Formation and identification of PAHs metabolites in marine organisms. Mar. Environ. Res. 91, 2–13.

Shelbourne, J.E., 1957. Site of chloride regulation in marine fish larvae. Nature 180, 920–922.

Shou, W., Aghdasi, B., Armstrong, D., Guo, Q., Bao, S., Charng, M., Mathews, L., Schneider, M., Hamilton, S., Matzuk, M., 1998. Cardiac defects and altered ryanodine receptor function in mice lacking FKBP12. Nature 391, 489–492.

Shwartz, Y., Farkas, Z., Stern, T., Aszodi, A., Zelzer, E., 2012. Muscle contraction controls skeletal morphogenesis through regulation of chondrocyte convergent extension. Dev. Biol. 370, 154–163.

Sievers, C.K., Shanle, E.K., Bradfield, C.A., Xu, W., 2013. Differential action of monohydroxylated polycyclic aromatic hydrocarbons with estrogen receptors alpha and beta. Toxicol. Sci. 132, 359–367.

Solemdal, P., Mukhina, N., Knutsen, T., Bjørke, H., Fossum, P., 1997. Maturation, Spawning and Egg Drift of Arcto-Norwegian Haddock (*Melanogrammus aeglefinus*), Icthyoplankt. Ecol. University college Galway, Ireland.

Sørensen, L., Sørhus, E., Nordtug, T., Incardona, J.P., Linbo, T.L., Giovanetti, L., Karlsen, O., Meier, S., 2017. Oil droplet fouling and differential toxicokinetics of polycyclic aromatic hydrocarbons in embryos of Atlantic haddock and cod. PLoS One 12, e0180048.

Sørensen, L., Hansen, B.H., Farkas, J., Donald, C.E., Robson, W.J., Tonkin, A., Meier, S., Rowland, S.J., 2019. Accumulation and toxicity of monoaromatic petroleum hydrocarbons in early life stages of cod and haddock. Environ. Pollut. 251, 212–220.

Sørhus, E., Edvardsen, R.B., Karlsen, O., Nordtug, T., van der Meeren, T., Thorsen, A., Harman, C., Jentoft, S., Meier, S., 2015. Unexpected interaction with dispersed crude oil droplets drives severe toxicity in Atlantic haddock embryos. PLoS One 10, e0124376.

Sørhus, E., Incardona, J.P., Karlsen, O., Linbo, T., Sørensen, L., Nordtug, T., van der Meeren, T., Thorsen, A., Thorbjørnsen, M., Jentoft, S., Edvardsen, R.B., Meier, S., 2016a. Crude oil exposures reveal roles for intracellular calcium cycling in haddock craniofacial and cardiac development. Sci. Rep. 6, 31058.

Sørhus, E., Incardona, J.P., Furmanek, T., Jentoft, S., Meier, S., Edvardsen, R.B., 2016b. Developmental transcriptomics in Atlantic haddock: illuminating pattern formation and organogenesis in non-model vertebrates. Dev. Biol. 411, 301–313.

Sørhus, E., Incardona, J.P., Furmanek, T., Goetz, G.W., Scholz, N.L., Meier, S., Edvardsen, R.B., Jentoft, S., 2017. Novel adverse outcome pathways revealed by chemical genetics in a developing marine fish. Elife 6.

Sun, L.B., Ruan, J.P., Lu, M.C., Chen, M., Dai, Z.L., Zuo, Z.H., 2019. Combined effects of ocean acidification and crude oil pollution on tissue damage and lipid metabolism in embryo-larval development of marine medaka (Oryzias melastigma). Environ. Geochem. Health 41, 1847–1860.

Ta, C.M., Adomaviciene, A., Rorsman, N.J., Garnett, H., Tammaro, P., 2016. Mechanism of allosteric activation of TMEM16A/ANO1 channels by a commonly used chloride channel blocker. Br. J. Pharmacol. 173, 511–528.

Thisse, C., Thisse, B., 2008. High-resolution in situ hybridization to whole-mount zebrafish embryos. Nat. Protoc. 3, 59–69.

Timme-Laragy, A.R., Noyes, P.D., Buhler, D.R., Di Giulio, R.T., 2008. CYP1B1 knockdown does not alter synergistic developmental toxicity of polycyclic aromatic hydrocarbons in zebrafish (Danio rerio). Mar. Environ. Res. 66, 85–87.

Valen, R., Eilertsen, M., Edvardsen, R.B., Furmanek, T., Ronnestad, I., van der Meeren, T., Karlsen, O., Nilsen, T.O., Helvik, J.V., 2016. The two-step development of a duplex retina involves distinct events of cone and rod neurogenesis and differentiation. Dev. Biol. 416, 389–401.

Van de Wiele, T., Vanhaecke, L., Boeckaert, C., Peru, K., Headley, J., Verstraete, W., Siciliano, S., 2005. Human colon microbiota transform polycyclic aromatic hydrocarbons to estrogenic metabolites. Environ. Health Perspect. 113, 6–10.

Vandenberg, J.I., Perry, M.D., Perrin, M.J., Mann, S.A., Ke, Y., Hill, A.P., 2012. hERG K^+ channels: structure, function, and clinical significance. Physiol. Rev. 92, 1393–1478.

Vanleeuwen, C.J., Griffioen, P.S., Vergouw, W.H.A., Maasdiepeveen, J.L., 1985. Differences in susceptibility of early life stages of rainbow-trout (Salmo-gairdneri) to environmental-pollutants. Aquat. Toxicol. 7, 59–78.

Vogel, C., Marcotte, E.M., 2012. Insights into the regulation of protein abundance from proteomic and transcriptomic analyses. Nat. Rev. Genet. 13, 227–232.

Wamhoff, B.R., Bowles, D.K., McDonald, O.G., Sinha, S., Somlyo, A.P., Somlyo, A.V., Owens, G.K., 2004. L-type voltage-gated Ca^{2+} channels modulate expression of smooth muscle differentiation marker genes via a Rho kinase/myocardin/SRF-dependent mechanism. Circ. Res. 95, 406–414.

Wamhoff, B.R., Bowles, D.K., Owens, G.K., 2006. Excitation-transcription coupling in arterial smooth muscle. Circ. Res. 98, 868–878.

Wang, Y., Pasparakis, C., Mager, E.M., Stieglitz, J.D., Benetti, D., Grosell, M., 2019. Ontogeny of urea and ammonia transporters in mahi-mahi (Coryphaena hippurus) early life stages. Comp. Biochem. Physiol. A Mol. Integr. Physiol. 229, 18–24.

Wells, P.G., Kim, P.M., Laposa, R.R., Nicol, C.J., Parman, T., Winn, L.M., 1997. Oxidative damage in chemical teratogenesis. Mutat. Res. 396, 65–78.

Wells, P.G., McCallum, G.P., Chen, C.S., Henderson, J.T., Lee, C.J.J., Perstin, J., Preston, T.J., Wiley, M.J., Wong, A.W., 2009. Oxidative stress in developmental origins of disease: teratogenesis, neurodevelopmental deficits, and cancer. Toxicol. Sci. 108, 4–18.

Williams, A.L., Eason, J., Chawla, B., Bohnsack, B.L., 2017. Cyp1b1 regulates ocular fissure closure through a retinoic acid-independent pathway. Invest. Ophth. Vis. Sci. 58.

Wincent, E., Jonsson, M.E., Bottai, M., Lundstedt, S., Dreij, K., 2015. Aryl hydrocarbon receptor activation and developmental toxicity in zebrafish in response to soil extracts containing unsubstituted and oxygenated PAHs. Environ. Sci. Technol. 49, 3869–3877.

Xu, E.G., Mager, E.M., Grosell, M., Pasparakis, C., Schlenker, L.S., Stieglitz, J.D., Benetti, D., Hazard, E.S., Courtney, S.M., Diamante, G., Freitas, J., Hardiman, G., Schlenk, D., 2016. Time- and oil-dependent transcriptomic and physiological responses to Deepwater Horizon oil in mahi-mahi (Coryphaena hippurus) embryos and larvae. Environ. Sci. Technol. 50, 7842–7851.

Xu, E.G., Magnuson, J.T., Diarnante, G., Mager, E., Pasparakis, C., Grosell, M., Roberts, A.P., Schlenk, D., 2018. Changes in microRNA-mRNA signatures agree with morphological, physiological, and behavioral changes in larval mahi-mahi treated with Deepwater Horizon oil. Environ. Sci. Technol. 52, 13501–13510.

Xu, E.G., Khursigara, A.J., Li, S.Y., Esbaugh, A.J., Dasgupta, S., Volz, D.C., Schlenk, D., 2019. mRNA-miRNA-Seq reveals neuro-cardio mechanisms of crude oil toxicity in red drum (Sciaenops ocellatus). Environ. Sci. Technol. 53, 3296–3305.

Xu, E.G.B., Mager, E.M., Grosell, M., Hazard, E.S., Hardiman, G., Schlenk, D., 2017. Novel transcriptome assembly and comparative toxicity pathway analysis in mahi-mahi (Coryphaena hippurus) embryos and larvae exposed to Deepwater Horizon oil. Sci. Rep. 7.

Yamamoto, Y., Zolfaghari, R., Ross, A.C., 2000. Regulation of CYP26 (cytochrome P450RAI) mRNA expression and retinoic acid metabolism by retinoids and dietary vitamin A in liver of mice and rats. FASEB J. 14, 2119–2127.

Yin, H.C., Tseng, H.P., Chung, H.Y., Ko, C.Y., Tzou, W.S., Buhler, D.R., Hu, C.H., 2008. Influence of TCDD on zebrafish CYP1B1 transcription during development. Toxicol. Sci. 103, 158–168.

Zimmer, A.M., Brauner, C.J., Wood, C.M., 2014. Ammonia transport across the skin of adult rainbow trout (Oncorhynchus mykiss) exposed to high environmental ammonia (HEA). J. Comp. Physiol. B. 184, 77–90.

Zimmer, A.M., Wright, P.A., Wood, C.M., 2017. Ammonia and urea handling by early life stages of fishes. J. Exp. Biol. 220, 3843–3855.